國立臺灣大學電機資訊學院資訊工程學研究所

博士論文

Department of Computer Science & Information Engineering

College of Electrical Engineering and Computer Science

National Taiwan University

Doctoral Dissertation

國立臺灣大學博士畢業論文

National Taiwan University (NTU)
Dissertation

盧與明

Yu-Ming Lu

指導教授: 呂育道 博士

Advisor: Yuh-Dauh Lyuu, Ph.D.

中華民國 114 年 12 月

December 2025

doi:10.5566/NTU2018XXXXX

國立臺灣大學博士學位論文

口試委員會審定書

國立臺灣大學博士畢業論文

National Taiwan University (NTU)
Dissertation

本論文係盧與明君（D08922008）在國立臺灣大學資訊工程學研究所完成之博士學位論文，於民國 114 年 12 月 16 日承下列考試委員審查通過及口試及格，特此證明

口試委員：_____

（指導教授）

_____ _____

_____ _____

_____ _____

_____ _____

所　　長：_____

doi:10.5566/NTU2018XXXXX

doi:10.5566/NTU2018XXXXX

Acknowledgements

常到外國朋友家吃飯。當蠟燭燃起，菜肴布好，客主就位，總是主人家的小男孩或小女孩舉起小手，低頭感謝上天的賜予，並歡迎客人的到來。

我剛到美國時，常鬧得尷尬。因為在國內養成的習慣，還沒有坐好，就開動了。

以後凡到朋友家吃飯時，總是先囑咐自己；今天不要忘了，可別太快開動啊！幾年來，我已變得很習慣了。但我一直認為只是一種不同的風俗儀式，在我這方面看來，忘或不忘，也沒有太大的關係。

前年有一次，我又是到一家去吃飯。而這次卻是由主人家的祖母謝飯。她雪白的頭髮，顫抖的聲音，在搖曳的燭光下，使我想起兒時的祖母。那天晚上，我忽然覺得我平靜如水的情感翻起滔天巨浪來。

在小時候，每當冬夜，我們一大家人圍著個大圓桌吃飯。我總是坐在祖母身旁。祖母總是摸著我的頭說：「老天爺賞我們家飽飯吃，記住，飯碗裡一粒米都不許剩，要是蹧蹋糧食，老天爺就不給咱們飯了。」

剛上小學的我，正在念打倒偶像及破除迷信等為內容的課文，我的學校就是從前的關帝廟，我的書桌就是供桌，我曾給周倉畫上眼鏡，給關平戴上鬍子，祖母的話，老天爺也者，我覺得是既多餘，又落伍的。

doi:10.5566/NTU2018XXXXX

不過，我卻很尊敬我的祖父母，因為這飯確實是他們掙的，這家確實是他們立的。我感謝面前的祖父母，不必感謝渺茫的老天爺。

這種想法並未因為年紀長大而有任何改變。多少年，就在這種哲學中過去了。

我在這個外國家庭晚飯後，由於這位外國老太太，我想起我的兒時，由於我的兒時，我想起一串很奇怪的現象。

祖父每年在「風裡雨裡的咬牙」，祖母每年在「茶裡飯裡的自苦」，他們明明知道要滴下眉毛上的汗珠，才能撿起田中的麥穗，而為什麼要謝天？我明明是個小孩子，混吃混玩，而我為什麼卻不感謝老天爺？

這種奇怪的心理狀態，一直是我心中的一個謎。

一直到前年，我在普林斯頓，瀏覽愛因斯坦的我所看見的世界得到了新的領悟。

這是一本非科學性的文集，專載些愛因斯坦在紀念會上啦，在歡迎會上啦，在朋友的喪禮中，他所發表的談話。

我在讀這本書時忽然發現愛因斯坦想盡量給聽眾一個印象：即他的貢獻不是源於甲，就是由於乙，而與愛因斯坦本人不太相干似的。

就連那篇亙古以來嶄新獨創的狹義相對論，並無參考可引，卻在最後天外飛來一筆，「感謝同事朋友貝索的時相討論。」

其他的文章，比如奮鬥苦思了十幾年的廣義相對論，數學部份推給了昔年好友的合作：這種謙抑，這種不居功，科學史中是少見的。

我就想，如此大功而竟不居，為什麼？像愛因斯坦之於相對論，像我祖母之

doi:10.5566/NTU2018XXXXX

於我家。

幾年來自己的奔波，做了一些研究，寫了幾篇學術文章，真正做了一些小貢獻以後，才有了一種新的覺悟：即是無論什麼事，得之於人者太多，出之於己者太少。因為需要感謝的人太多了，就感謝天罷。無論什麼事，不是需要先人的遺愛與遺產，即是需要眾人的支持與合作，還要等候機會的到來。越是真正做過一點事，越是感覺自己的貢獻之渺小。

於是，創業的人，都會自然而然的想到上天，而敗家的人卻無時不想到自己。

doi:10.5566/NTU2018XXXXX

doi:10.5566/NTU2018XXXXX

摘要

中文摘要

關鍵字： LaTeX、中文、論文、模板

doi:10.5566/NTU2018XXXXX

doi:10.5566/NTU2018XXXXX

Abstract

The implied barrier is the barrier that yields a default probability or reproduces a barrier option price. This thesis proposes a highly efficient algorithm based on the Black-Scholes model to find the implied barrier and proves its convergence rate. In particular, it presents an $O(n \log n)$-time tree algorithm to find the implied step barrier, where n denotes the tree's number of time steps. Our algorithm is one order faster than the standard tree algorithm. This algorithm can be easily adapted to obtain the implied barrier when it is defined at discrete points, or to price various types of barrier options with accuracy. For the case of a constant barrier, the implied barrier is proved to converge to its true value at a rate of $O(n^{-1})$. Numerical experiments confirm this rate. The experiments also show that the implied step barrier converges at the same rate. The implied barrier can be seen as the default boundary that reproduces the default probabilities under a structural model. When the default probabilities are obtained from publicly available data, the implied barrier reflects the market consensus. Finally, we propose (1) a new binary default

doi:10.5566/NTU2018XXXXX

prediction scheme for publicly listed corporations and (2) a new evaluation scheme for binary default prediction schemes. The results show good performance for publicly listed U.S. companies during 1991–2023.

Keywords: LaTeX, CJK, Thesis, Template

doi:10.5566/NTU2018XXXXX

Contents

doi:10.5566/NTU2018XXXXX

doi:10.5566/NTU2018XXXXX

doi:10.5566/NTU2018XXXXX

doi:10.5566/NTU2018XXXXX

List of Figures

doi:10.5566/NTU2018XXXXX

doi:10.5566/NTU2018XXXXX

doi:10.5566/NTU2018XXXXX

doi:10.5566/NTU2018XXXXX

List of Tables

doi:10.5566/NTU2018XXXXX

doi:10.5566/NTU2018XXXXX

Chapter 1: Introduction

1.1 Background and Motivations

Many real-world systems operate under uncertainty and often exhibit significant changes when certain thresholds are crossed. These thresholds can mark the transition from normalcy to failure, from equilibrium to instability, or from solvency to insolvency. When such thresholds are exerted over a period of time, either continuously or at discrete time points, they are called barriers. Barriers play a critical role in understanding the dynamics of real-world systems because they govern when and how significant changes occur abruptly (see [77] and [78]). When barriers are latent, accurately and efficiently obtaining them is essential to preventing irreversible system transitions, supporting early-warning mechanisms, and enhancing overall decision-making under uncertainty.

This thesis focuses on barriers in credit analysis (see [34] and [54]). Specifically, we examine the barrier that separates a company's creditworthy status from the onset of a credit event. It is called the default boundary. In practice, the default boundary itself is not directly observable (see [27]). Instead, financial indicators such as asset value, leverage ratio, or working capital are commonly monitored for deteriorating financial conditions (see [2]). When an indicator falls to a critical level, the company may become unable to meet its obligations, resulting in a credit event. For instance, a significant decrease

doi:10.5566/NTU2018XXXXX

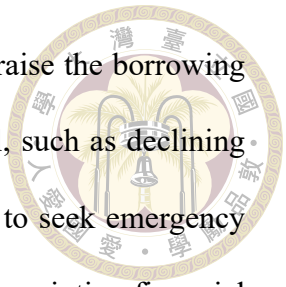

in asset value relative to debt can weaken creditors' confidence and raise the borrowing cost. As another example, a substantial reduction in working capital, such as declining cash reserves or rising short-term payables, may force the company to seek emergency funding under unfavorable terms. These scenarios illustrate how disappointing financial indicators can lead to deteriorating credit quality, which may result in credit events such as debt restructuring or even bankruptcy. In such cases, the default boundary is crossed.

A company's default boundary is heavily influenced by its liability structure, which involves many kinds of obligations such as debt, taxes, and accounts payable (see [61]). Straight bonds have clear payment schedules and fixed maturity dates. If a company's cash is insufficient to meet the required payments, default can occur. Debts with embedded options or redemption features do not even have well-defined maturities, which introduces uncertainty about the timing and size of future obligations (see [46]). Debt issues furthermore interact with each other to complicate the default boundary (see [84]). As for taxes, a change in corporate tax rates can significantly alter the present value of the interest-tax shield and therefore affect a company's leverage ratio (see [38]). Altogether, these factors show how a company's liability structure influences its default boundary.

The default boundary can also be influenced by strategic considerations. Theoretically, a company is considered solvent if its assets exceed its liabilities because it can, in principle, liquidate its assets to repay its liabilities. But a company's equity holders may choose to default strategically even when the company's assets suffice to cover its liabilities (see [5]). This is because default may confer certain advantages over the repayment of debts. For example, when a company is in distress, the equity holders may threaten to file for bankruptcy in order to renegotiate the terms of its debt. While debt holders are eligible to seize the company's assets upon default, this process is costly and time-consuming,

doi:10.5566/NTU2018XXXXX

which weakens the debt holders' bargaining position. As a result, the equity holders may be able to negotiate a lower interest rate or even a partial cancellation.

Given that the default boundary is not directly observable and is influenced by multiple interacting factors, inferring this boundary from data becomes an attractive alternative (see [9] and [45]). The resulting default boundary is called the implied barrier by [18], which is the main topic of this thesis. When the implied barrier is obtained from publicly available data, it reflects market consensus. This thesis will obtain the implied barrier from publicly available default probabilities, which refer to the probabilities that a company will default over periods of time. Specifically, the implied barrier is the default boundary that reproduces the default probabilities under a structural model.

Structural models are a class of credit risk models based on the option-pricing framework; as a result, corporate securities are contingent claims on a company's assets (see [54]). While initially developed to price corporate liabilities, structural models offer an economic framework for credit analysis. These models make three assumptions: (1) the company's asset value follows a stochastic process, (2) default occurs if the asset value drops to a default boundary, and, if implicitly, (3) the default boundary is a function of asset value and time.

The first structural model is proposed by [69]. He assumes a company's asset value follows a geometric Brownian motion and that it has only zero-coupon bonds (ZCBs) with the same maturity as the liabilities. In Merton's model, default occurs when the asset value falls to the total face value of the ZCBs at their maturity. The framework can be extended to any debt structure in principle.

In reality, companies can default anytime, contrary to Merton's assumption. [12] ad-

doi:10.5566/NTU2018XXXXX

dress this issue by proposing a first-passage-time structural model. They specify default as the first time the asset value touches the default boundary. Like Merton, they assume the company holds same-maturity ZCBs but now with safety covenants. The covenants provide bondholders with the right to initiate bankruptcy proceedings or enforce a reorganization if they are violated. Therefore, the safety covenants give rise to the default boundary.

The determination and, when applicable, the functional form of the default boundary play a critical role in structural models. Before delving into our approach, it is useful to examine how default boundaries are typically handled within structural models. One common approach is to consider the book value of the outstanding liabilities and assume a parametric form. The simplest form is a constant default boundary (see [51], [58], [18], and [25]). However, a constant default boundary can be internally inconsistent. Consider $p(t_1)$ and $p(t_2)$ as the cumulative probabilities of a company defaulting at or before times t_1 and t_2, respectively, where $t_1 < t_2$. They are likely to result in two different levels of default boundary b_1 and b_2, respectively, where b_1 covers the time from now through t_1 whereas b_2 covers the time from now through the later t_2. So the period from now to time t_1 is associated with two different levels. Other than the constant default boundary, the exponential default boundary is also popular (see [12], [63], and [85]). Instead of assuming a parametric form, [4] apply game theory to endogenously determine the default boundary. Their default boundary is the equilibrium of a game in which equity holders and debt holders interact strategically.

As mentioned above, this thesis infers the default boundary from publicly available default probabilities under a structural model; this boundary is the implied barrier. We define the default probability over the time horizon $(0, T]$ as the probability of the com-

doi:10.5566/NTU2018XXXXX

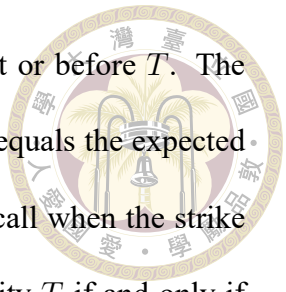

pany's asset value, starting above the boundary, hitting the barrier at or before T. The survival probability, which equals one minus the default probability, equals the expected payoff of a special barrier option: The down-and-out digital barrier call when the strike price equals the barrier (DODC). A DODC pays one dollar at maturity T if and only if the underlying asset's price never touches the barrier by T. Throughout this thesis, the underlying asset is assumed to be a stock, except in Chapter 5.

As there are no closed-form formulas for the implied barrier, any numerical methods to find it must repeatedly calculate the expected payoff of a DODC and compare it against the target survival probability until the difference is acceptably small. When the barrier is a constant, the expected payoff can be easily calculated through a closed-form formula (see [74]). However, when the barrier has a more complex form, such as a step function, the closed-form formula is hard to compute in general as it involves a multiple integral (see [57]). We adopt tree algorithms to compute the expected payoff of the DODC with a step barrier because they are efficient. This thesis focuses on the step-barrier case because a step barrier can approximate any continuous barrier.

With the implied barrier in place, we can apply it to corporate default prediction. The task is to identify whether a company will experience a credit event within a time horizon. The importance of having an effective default prediction scheme is self-evident: The cost of default can be high. For example, in 2007, "irrational exuberance" in the market led to an underestimation of default risk and resulted in the overpricing of such derivatives as collateralized debt obligations (CDOs) (see [80]). This became a crucial factor in the ensuing global financial crisis and cost more than a trillion dollars in national output (see [8] and [70]).

doi:10.5566/NTU2018XXXXX

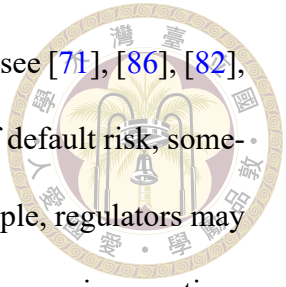

Typical default prediction schemes provide default probabilities (see [71], [86], [82], [21], and [19]). While they can be used to rank companies in terms of default risk, sometimes a binary classification is needed for decision-making. For example, regulators may need to classify banks as either at risk of failure or not before taking supervisory actions (see [68]). Of course, a default probability can be converted into a binary prediction, i.e., default or no-default, by applying a cutoff threshold. The threshold may be chosen in an ad hoc manner (often 0.5) or based on some principles (see [71], [86], [72], and [10]).

Unlike thresholds, the implied barrier provides an alternative way to turn default probabilities into binary default predictions. It is furthermore economically reasonable. The idea is to compare the company's future expected asset value with the implied barrier. Default is predicted if and only if the expected asset value ever touches the implied barrier. Since the implied barrier is inferred from default probabilities, which in turn rely on market and accounting data, our scheme focuses on publicly listed companies, for which such information is available. Finally, this thesis proposes a new scheme to evaluate the performance of binary default prediction schemes.

1.2 Literature Review

1.2.1 Algorithms for Implied Barrier

In structural models, the default probability is equivalent to the probability of the company's asset value hitting the barrier from above, i.e., the barrier-hitting probability. Moreover, the barrier-hitting probability equals one minus the DODC's expected payoff. An option's expected payoff is closely related to its price: The expected payoff is

doi:10.5566/NTU2018XXXXX

computed under the real-world measure, while the option price is evaluated under the risk-neutral measure and involves discounting. Thus, if one can compute one, one can compute the other with the same computational time.

A common approach to inferring the implied barrier is to numerically invert closed-form formulas for either the barrier-hitting probability or the barrier option price. Under the Black and Scholes's (BS) (1973) model, formulas for the barrier-hitting probability are available for the constant-barrier case (see [47]) and the step-barrier case (see [57]). Formulas for the barrier option price are available for the cases of constant barrier (see [69] and [73]), discrete constant barrier (see [17] and [52]), partial and window constant barriers (see [40], [43], and [6]), piecewise exponential barrier (see [53]), step barrier (see [57]), continuously differentiable barrier (see [76]), and a mixture of continuously and discretely monitored barrier (see [22]). Note that any barrier that is not constant can be viewed as a time-varying barrier, which is also called a moving barrier in this thesis. Figure 1.1 shows five common types of barriers.

Recall that we focus on the step-barrier case because a step barrier can approximate any continuous barrier. Formulas for step-barrier options involve multiple integrals ([57]). Extracting the implied barrier from them is infeasible because the computational cost grows exponentially in the dimension. Monte Carlo simulation is also not recommended for obtaining the implied barrier because of its (1) stochastic and moderately large error, and (2) relative inefficiency. A general and efficient alternative is thus desirable for finding the implied step barrier. This thesis focuses on trees as a solution.

Trees are commonly used to price financial derivatives when closed-form formulas are unavailable or too costly to evaluate (see [65]). A tree discretizes the continuous pro-

doi:10.5566/NTU2018XXXXX

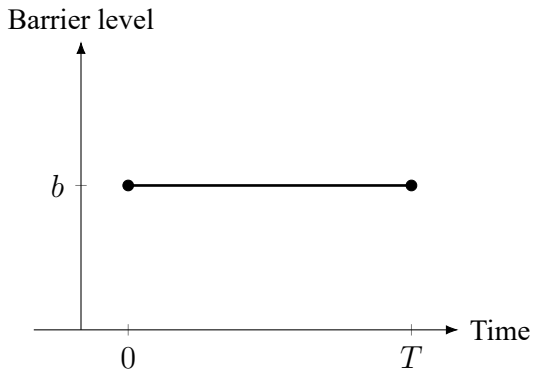

(a) Constant barrier.

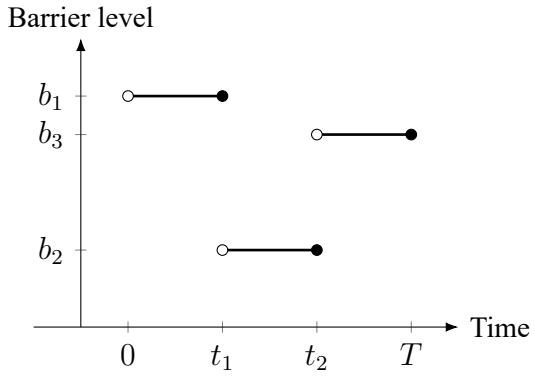

(b) 3-step barrier.

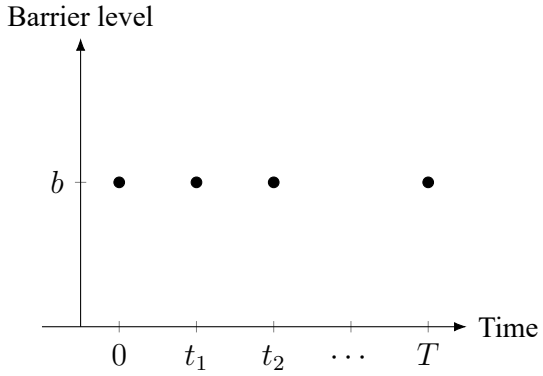

(c) Discrete constant barrier.

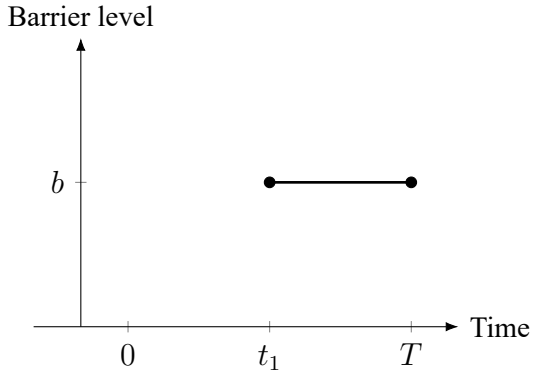

(d) Partial constant barrier.

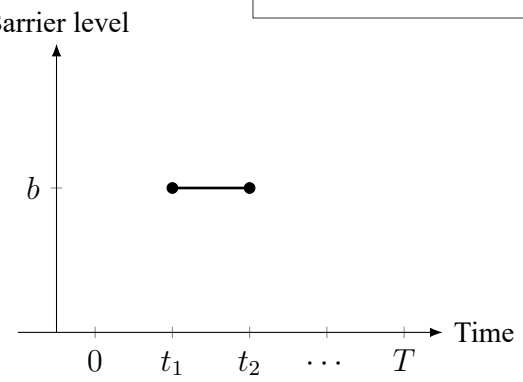

(e) Window constant barrier.

Figure 1.1: Popular barrier types. t_is are the monitoring points and T is the maturity date.

cess of the stock price. A properly calibrated tree converges to the continuous-time model as n increases, where n is the tree's number of time steps (see [31]). Cox, Ross, and Rubinstein (CRR) (1979) propose the first tree based on the BS model, known as the CRR tree. It can be used to price various kinds of options. For example, the prices of a vanilla call by the CRR tree are shown in Figure 1.2. They clearly converge to the true value given by the BS formula.

doi:10.5566/NTU2018XXXXX

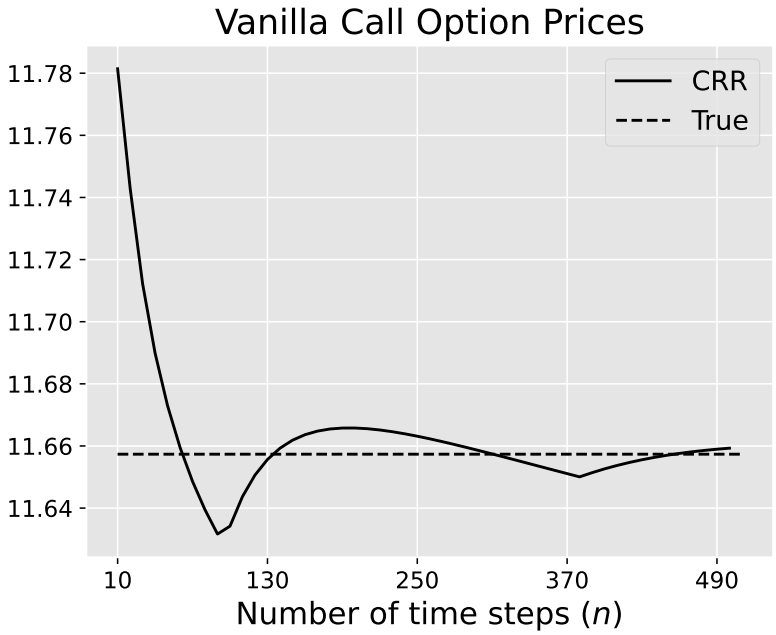

Figure 1.2: The vanilla call prices by the CRR tree for $n = 10, 20, 30, \ldots, 500$. The dashed line 11.6573 gives the true value by the BS formula.

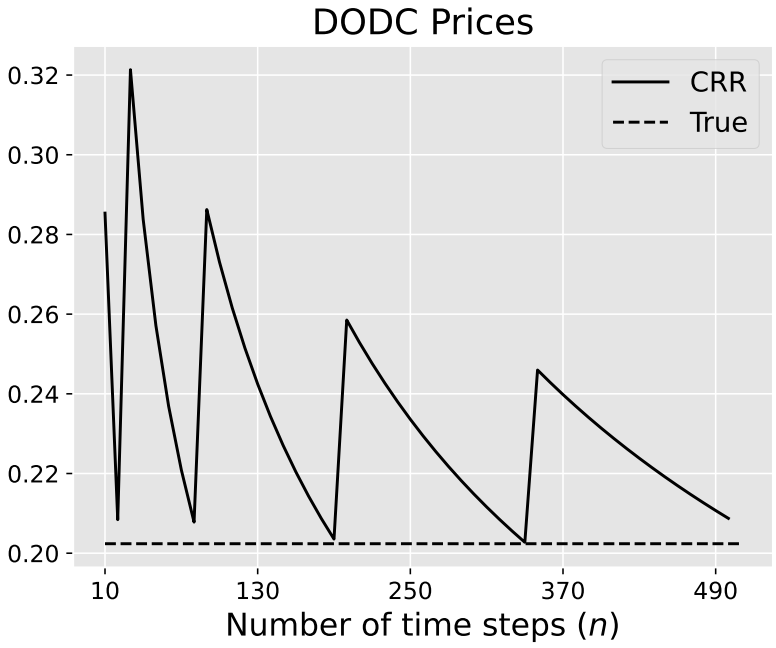

Figure 1.3: The DODC prices by the CRR tree for $n = 10, 20, 30, \ldots, 500$. The dashed line 0.2023 gives the true value by Reiner and Rubinstein's (1991) formula.

The CRR tree has its drawbacks. When pricing barrier options in particular, the CRR tree produces large oscillations, meaning slow convergence. This is caused mostly by the misalignment between the barrier and the tree nodes, resulting in the nonlinearity error (see [36]). Figure 1.3 illustrates this problem when pricing a DODC.

doi:10.5566/NTU2018XXXXX

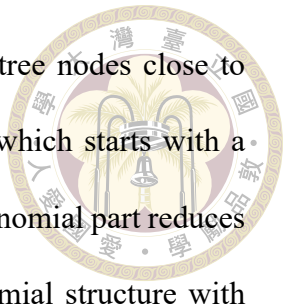

[16] and [75] reduce the nonlinearity error by placing critical tree nodes close to or on the barrier. [26] propose the binomial-trinomial tree (BTT), which starts with a trinomial structure and continues on with a binomial structure. The trinomial part reduces the nonlinearity error by aligning one of the tree levels in the binomial structure with the barrier. The subsequent binomial part enables the use of fast combinatorial formulas (see [64]) and the fast Fourier transform (FFT) (see Chapter 3).

1.2.2 Convergence Rates for Trees

With trees, the implied barrier is determined by iteratively adjusting the barrier level to match a target value such as the barrier-hitting probability or the option's expected payoff. The efficiency of this process depends on how quickly the algorithm computes the relevant quantity and compares it with the target value, and on how rapidly the iterative procedure converges.

[24] not only propose the CRR tree to price options but also demonstrate its convergence to the BS model. However, they do not address the convergence rate. [83] and [20] prove a linear convergence rate for the vanilla European option price by the CRR tree. [55] prove a quadratic convergence rate for the vanilla option price by the CRR tree after Richardson's extrapolation is applied. [56] derive the convergence rates for European path-independent options by binomial, trinomial, and m-nomial trees. [59] prove a linear convergence rate for the European barrier call price given by the CRR tree when (1) the barrier is aligned with one of the tree levels and (2) the strike price is equal to the barrier. The CRR tree is unable to align with the barrier in general, in which case the nonlinearity error makes the convergence erratic and slower than linear, as shown in Figure 1.3.

doi:10.5566/NTU2018XXXXX

1.2.3 Application to Default Prediction

[29] famously opines that "forecasting is not a respectable human activity and not worthwhile beyond the shortest of periods." This thesis will not contest the statement in the case of predicting company default; an almost perfect predictor for that task is neither our goal nor feasible. Instead, we believe publicly available financial data, by constraining how the future unfolds, already afford us very good guidance in predicting company default within, say, the next 5 years.

Default models can be used to price corporate debts or monitor the health of financial entities such as banks and pension funds (see [82]). A model that can predict the default event of a financial entity with reasonable accuracy narrows the information asymmetry between investors and management. A good model may even spot profitable opportunities.

Empirical analysis of default becomes active in the 1960s. [11] and [2] apply discriminant analysis to accounting and economic ratios to gauge whether a company is financially sound. [71] and [86] frame the problem with a logit model. For convenience, we refer to the above models as the traditional models. The advantage of traditional models is the transparent relation between the explanatory variables and the likelihood of default (see [3]). However, accounting data, being mostly backward looking, will obviously be strained in predicting future defaults (see [41]). [82] refers to traditional models as static models because they are time independent. These models rely on financial indicators from a single period only, and therefore ignore companies' performance over time. As a result, they might produce biased predictor variables and thus overlook default companies that had unfavorable indicators in periods other than the one used in estimation. Outside those

doi:10.5566/NTU2018XXXXX

traditional approaches, default models can be grouped into two categories: reduced-form models and structural models.

Reduced-form models characterize the default event by an exogenous point process in which the default time is the first jump time of the process (see [34]). Initially, they focus on pricing corporate bonds by specifying, explicitly or tacitly, a default intensity process and a recovery rate process (see [60], [49], [48], and [33]). The default intensity gives rise to the default probabilities. The recovery rate refers to the residual proportion of a financial entity because investors are entitled to the remaining value after bankruptcy. The default probabilities from reduced-form models have later been applied to default prediction. [82], [21], [19], and [15] use hazard models to obtain default probabilities. [32] specify a doubly-stochastic formulation of the point process for defaults and other types of firm exits caused by, for example, leveraged buyout, seizure by regulator, delisting, or merger and acquisition. [30] propose a forward intensity approach to tackle the high-dimensional problem in [32] and make the implementation more efficient.

Since the default event is triggered externally, reduced-form models lack an intuitive explanation of default. In contrast, in structural models, default occurs when the company's asset value hits the default boundary from above (recall Section 1.1). This means the default event is determined endogenously by the company's financial status. This thesis adopts the structural models because they offer an intuitive explanation of default events and provide a framework to explicitly talk about the default boundary.

doi:10.5566/NTU2018XXXXX

1.3 Contributions

The contributions of this thesis are as follows. First, we propose a highly efficient $O(n \log n)$-time tree algorithm based on the BS model to obtain the implied barrier, where n denotes the tree's number of time steps. We call it the core algorithm. When compared with the standard implementation, the core algorithm is at least an order faster. The core algorithm finds the exact implied barrier for a tree from the barrier-hitting probabilities when the barrier is a step function. The implied barrier is exact in the sense that it reproduces the barrier-hitting probabilities for any $n \geq 1$. For simplicity, we omit the term "exact" in the thesis unless emphasis is required. In the simplest constant-barrier case, the implied barrier is close to the true barrier even with small n's. Indeed, using $n = 1$ and $n = 3$ for extrapolation typically suffices to closely approximate the true barrier.

Second, we prove that the implied barrier by our core algorithm converges to its true value at a rate of $O(n^{-1})$ when the barrier is a constant. The numerical results suggest the same convergence rate holds when the barrier is a step function.

Finally, we propose a binary default prediction scheme under structural models as an application of the implied barrier. The core algorithm's accuracy and super efficiency are the keys to handling this task because the dataset is huge. Moreover, we propose a new scheme to evaluate binary default prediction schemes. The results suggest that the implied barrier performs well in predicting corporate defaults for companies listed on U.S. exchanges.

The remainder of this thesis is structured as follows. Chapter 2 introduces the preliminaries and notations used throughout the thesis. Chapter 3 presents the proposed tree

doi:10.5566/NTU2018XXXXX

algorithm for finding the implied barrier and its adaptations for option pricing. Chapter 4 provides the mathematical proof of the linear convergence rate of the implied barrier. Chapter 5 explores the practical applications of the implied barrier in corporate default prediction.

doi:10.5566/NTU2018XXXXX

Chapter 2: Preliminaries

This chapter introduces the fundamental concepts relevant to our thesis. Section 2.1 defines term sturcture of default probabilites. Section 2.2 describes risk-neutral option pricing. Section 2.3 introduces barrier options. Section 2.4 explains the reflection principle on a binomial random walk. Section 2.5 discusses the CRR tree. Section 2.6 elaborates on the binomial-trinomial tree, which forms the computational structure of the thesis.

2.1 Term Structure of Default Probabilities

Define τ as a nonnegative random variable representing a company's default time in the future. The term structure of default probabilities is the function

$$p(t \mid t_0) = \Pr(\tau \leq t_0 + t \mid t_0),$$

the cumulative probability of defaulting at or before time t, observed at time t_0 when the company is not in default (see [54] and [14]). We refer to t_0+t as the monitored time point. For simplicity, we will omit the term "cumulative" and call $p(t \mid t_0)$ the default probability over the time interval $(\, t_0, t_0 + t \,]$.

doi:10.5566/NTU2018XXXXX

2.2 Risk-Neutral Pricing

Risk-neutral pricing is critical to pricing financial derivatives like options. It says the price of a derivative equals its expected payoff discounted at the risk-free interest rate (see [44]). In other words, given a payoff C_T at maturity T, its theoretical price C_0 now equals

$$C_0 = e^{-rT} E^Q \left[C_T \right], \tag{2.1}$$

where $E^Q[\,\cdot\,]$ is the expectation under the risk-neutral probability measure Q.

In the BS model, a stock price S follows a geometric Brownian motion under the real-world probability measure P:

$$dS \;=\; \mu S dt + \sigma S \, dW^P, \tag{2.2}$$

where μ is the the growth rate of the stock price return, σ is the volatility, and W^P is the Wiener process under the P measure. By Ito's lemma, process (2.2) becomes

$$d\log S \;=\; \left(\mu - \frac{\sigma^2}{2} \right) dt + \sigma \, dW^P \tag{2.3}$$

(see [81]).

Under the Q measure, where all assets are expected to grow at the risk-free interest rate r, process (2.3) becomes

$$d\log S \;=\; \left(r - \frac{\sigma^2}{2} \right) dt + \sigma \, dW^Q,$$

where W^Q is the Wiener process under the Q measure.

doi:10.5566/NTU2018XXXXX

2.3 Barrier Option

A barrier option is a vanilla option plus a barrier that triggers a specific event. Its payoff depends on whether the underlying stock's price reaches a given level at any time before maturity. Depending on the barrier type, the option can be activated (the knock-in type) or terminated (the knock-out type) when the barrier is touched. We focus on the latter case. The most basic example is the down-and-out call (DOC). A DOC is terminated if the barrier is touched by the underlying stock's price from above. The payoff of a typical DOC is therefore

$$C_T^{\text{DOC}} = \max\left(S_T - K, 0\right) \mathbb{1}\left[\!\left[S_t > B_t \quad \text{for all } t \in [\,0, T\,] \right]\!\right], \tag{2.4}$$

where S_t is the stock price at time t, K is the strike price, B_t is the barrier at time t, and $\mathbb{1}$ is the indicator function. The DODC mentioned in Section 1.1 has a similar but simpler payoff:

$$C_T^{\text{DODC}} = \mathbb{1}\left[\!\left[S_t > B_t \quad \text{for all } t \in [\,0, T\,] \right]\!\right].$$

2.4 The Reflection Principle

A lattice consists of rectangular lines. The intersection of two lines defines a lattice point. A binomial random walk on the lattice allows a move from position (i, j) to $(i + 1, j + 1)$ or $(i + 1, j - 1)$ per step. We now count the number of walks that start from $(0, u)$ and end at (n, v) while hitting the x-axis in the process. The reflection principle says that number equals the number of walks from $(0, -u)$ to (n, v) when $n - u - v$ is even and $u > 0$. This is because reflecting the part of the walk before it touches the x-axis for the

doi:10.5566/NTU2018XXXXX

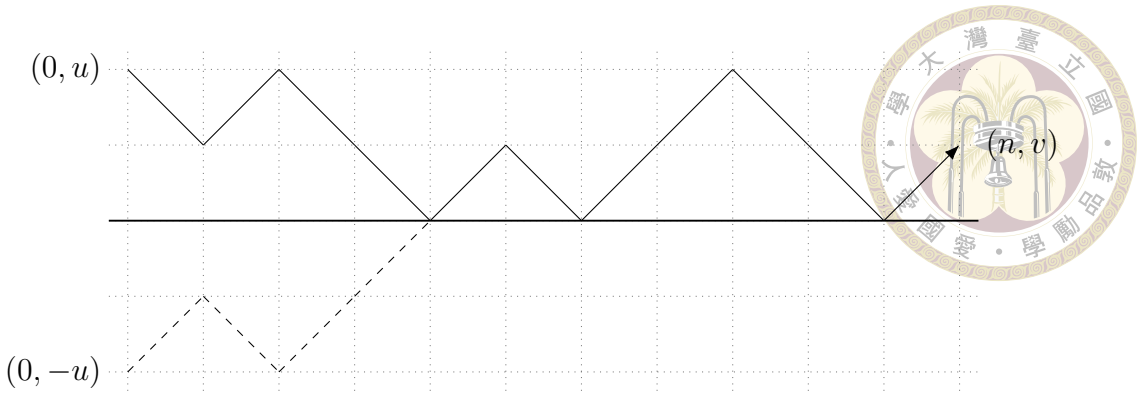

Figure 2.1: The reflection principle. The thick horizontal line denotes the x-axis.

first time yields a walk from $(0, -u)$ in a one-to-one manner (see Figure 2.1). Because such walks must contain $v + u$ more up moves than down moves in n steps, the desired count totals

$$\frac{n!}{[\,(n+u+v)/2\,]!\,[\,(n-u-v)/2\,]!} = \binom{n}{\frac{n-u-v}{2}} \tag{2.5}$$

and zero when $n - u - v < 0$ or $n - u - v > n$ (see [64]).

2.5 The CRR Tree

Assume the logarithmic stock price follows process (2.3). A binomial tree discretizes process (2.3) from t to T by dividing it evenly into n time steps; thus each time step has a duration of $\Delta t \equiv (T - t)/n$. The logarithmic stock price $\log S$ can either go upward to $\log S + \log u$ with probability p or downward to $\log S + \log d$ with probability $1 - p$ per step, where u, d, and p are chosen to match the mean and variance of process (2.3) asymptotically. These parameters are chosen by the CRR to be $u \equiv e^{\sigma\sqrt{\Delta t}}$, $d \equiv e^{-\sigma\sqrt{\Delta t}}$, and $p \equiv (e^{\mu\Delta t} - d)/(u - d)$. They are attractive because the property $ud = 1$ is convenient for our base case, where the barrier is a constant barrier or a step function. Figure 2.2 illustrates a CRR tree for $n = 2$. Note that the spacing between two vertically adjacent nodes is $2\sigma\sqrt{\Delta t}$. For the risk-neutral measure needed for options pricing, simply set

doi:10.5566/NTU2018XXXXX

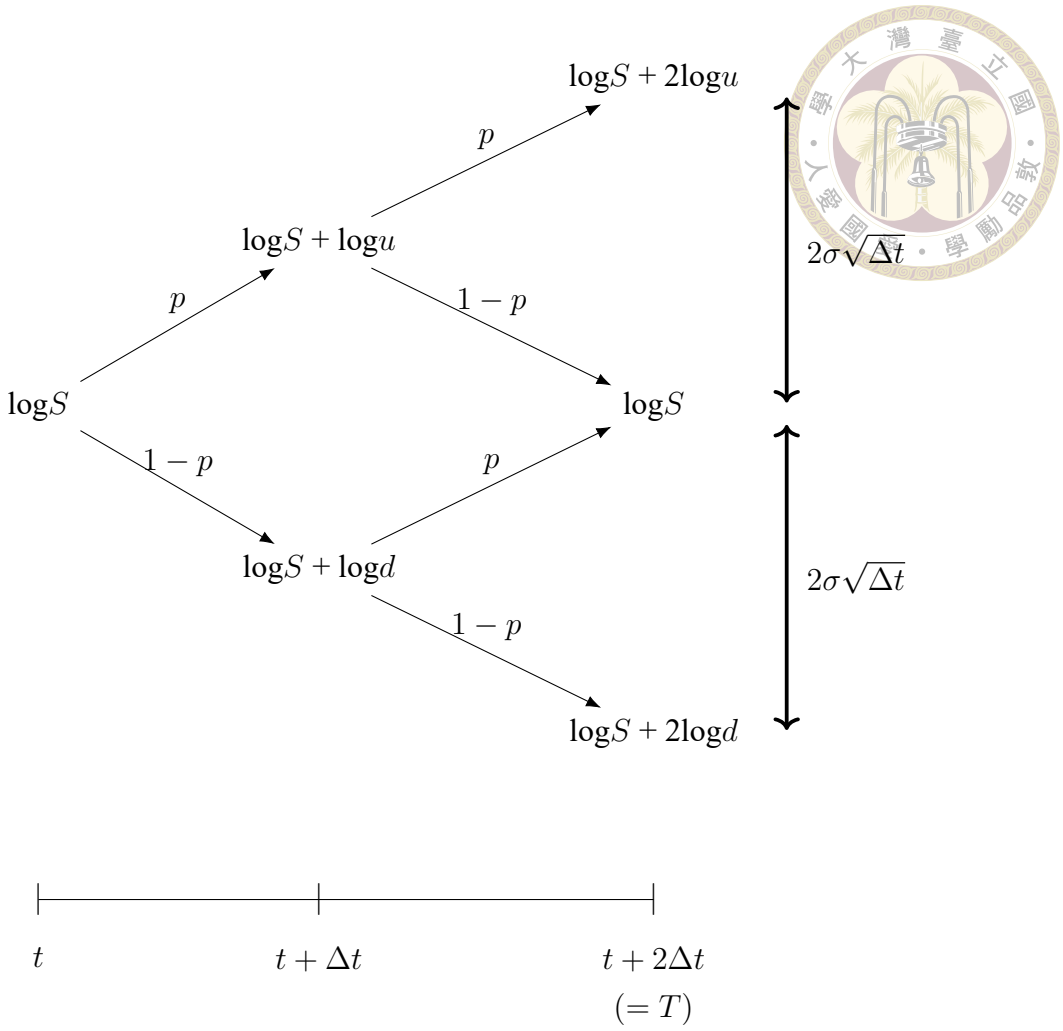

Figure 2.2: A CRR tree for $n = 2$.

$\mu = r$, the risk-free interest rate.

The growth rate and the volatility in process (2.3) are constants. In more general models, these parameters can be functions of time, denoted by $\mu(t)$ and $\sigma(t)$ (see [66]).

2.6 The Binomial-Trinomial Tree

A binomial-trinomial tree (BTT) starts with a trinomial structure in the first time step and continues on with a binomial one. Below, we illustrate how to construct a BTT with a barrier b in logarithm from t to T with reference to Figure 2.3. First, lay down the lattice underlying the binomial structure, where one of the horizontal lines is aligned with b. The

doi:10.5566/NTU2018XXXXX

horizontal lines of the lattice are equispaced at $\sigma\sqrt{\Delta t}$ apart. Let s_z denote the logarithmic stock price of node z and define $s_{\mathrm{X}} - s_{\mathrm{Y}}$ as the logarithmic return from node X to node Y. Define $\theta \equiv (\mu - \sigma^2/2)\,\Delta t$ as the expected logarithmic return for continuous-time model (2.3) at time Δt. The trinomial structure for the first time step at the root node R is built as follows. Name R's top, middle, and bottom successor nodes A, B, and C, respectively. Place node B on the grid point at time Δt so that $\hat{\theta} \equiv s_{\mathrm{B}} - s_{\mathrm{R}}$ is closest to θ, breaking ties in favor of the lower node. Place node A (node C) $2\sigma\sqrt{\Delta t}$ higher (lower, resp.) than node B.

Define

$$\alpha \equiv \hat{\theta} - \theta + 2\sigma\sqrt{\Delta t}, \tag{2.6}$$

$$\beta \equiv \hat{\theta} - \theta, \tag{2.7}$$

$$\gamma \equiv \hat{\theta} - \theta - 2\sigma\sqrt{\Delta t} \tag{2.8}$$

(see Figure 2.4). Because the horizontal lines are $\sigma\sqrt{\Delta t}$ apart, we have

$$-\sigma\sqrt{\Delta t} \le \beta \le \sigma\sqrt{\Delta t}. \tag{2.9}$$

After the trinomial structure is established, grow a binomial structure from nodes A, B, and C at time Δt through time T on the underlying grid (see Figure 2.3). Note that the position of node B can be written as $b + i^*\,\sigma\sqrt{\Delta t}$ where

$$i^* = \operatorname*{argmin}_{i \in Z} \left| b + i\,\sigma\sqrt{\Delta t} - \theta \right|$$

and, in case the minimum value is reached at two is, the lower i is chosen because the algorithm breaks ties in favor of the lower node.

doi:10.5566/NTU2018XXXXX

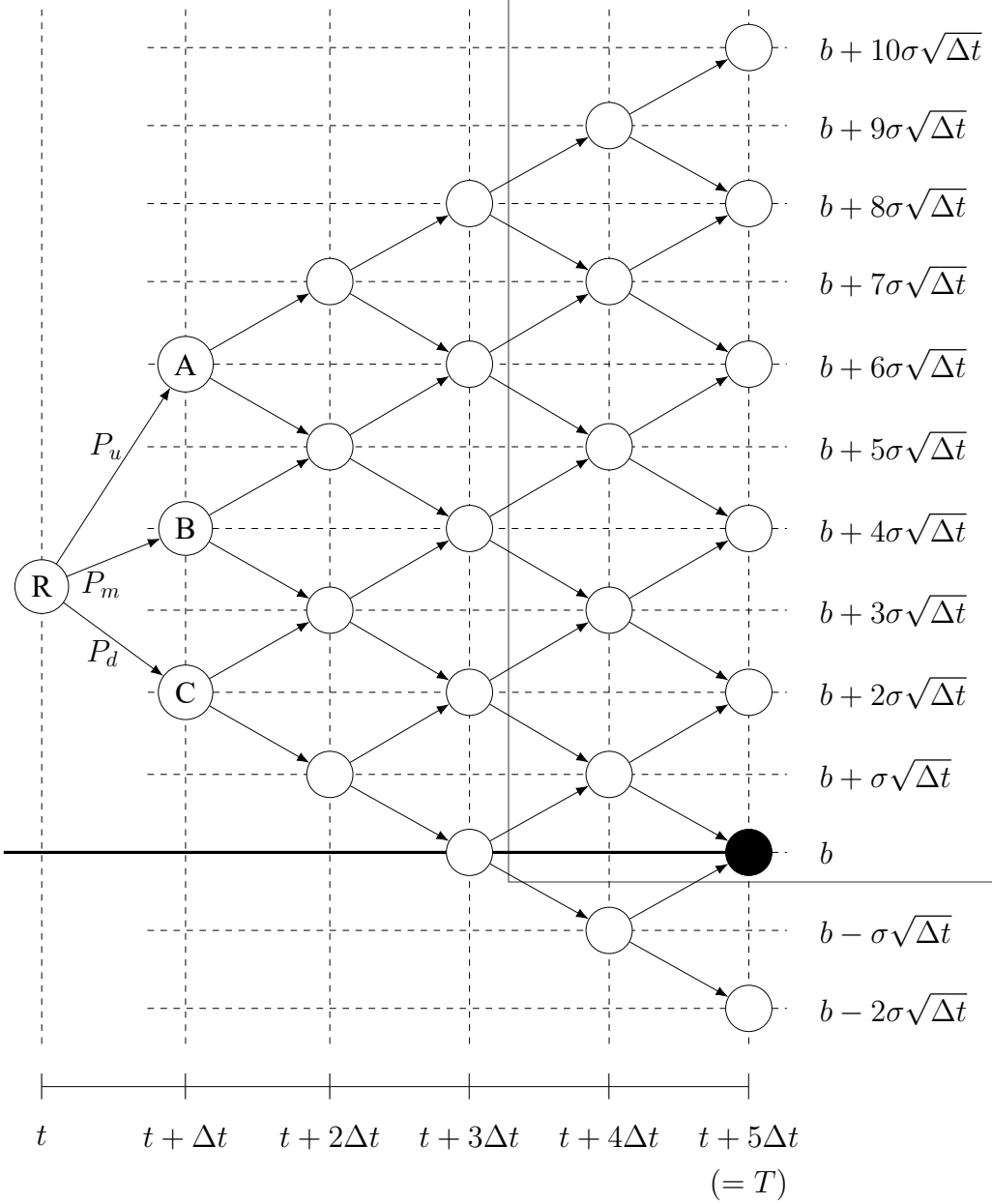

Figure 2.3: A BTT with a barrier b. It starts with a trinomial structure. The part after time $t + \Delta t$ features a binomial structure.

Obtain the branching probabilities by solving the following linear equations:

$$P_u\alpha + P_m\beta + P_d\gamma = 0, \tag{2.10}$$

$$P_u\alpha^2 + P_m\beta^2 + P_d\gamma^2 = \text{Var}, \tag{2.11}$$

$$P_u + P_m + P_d = 1, \tag{2.12}$$

where $\text{Var} \equiv \sigma^2\Delta t$ is the variance of the logarithmic return after Δt time under the pro-

doi:10.5566/NTU2018XXXXX

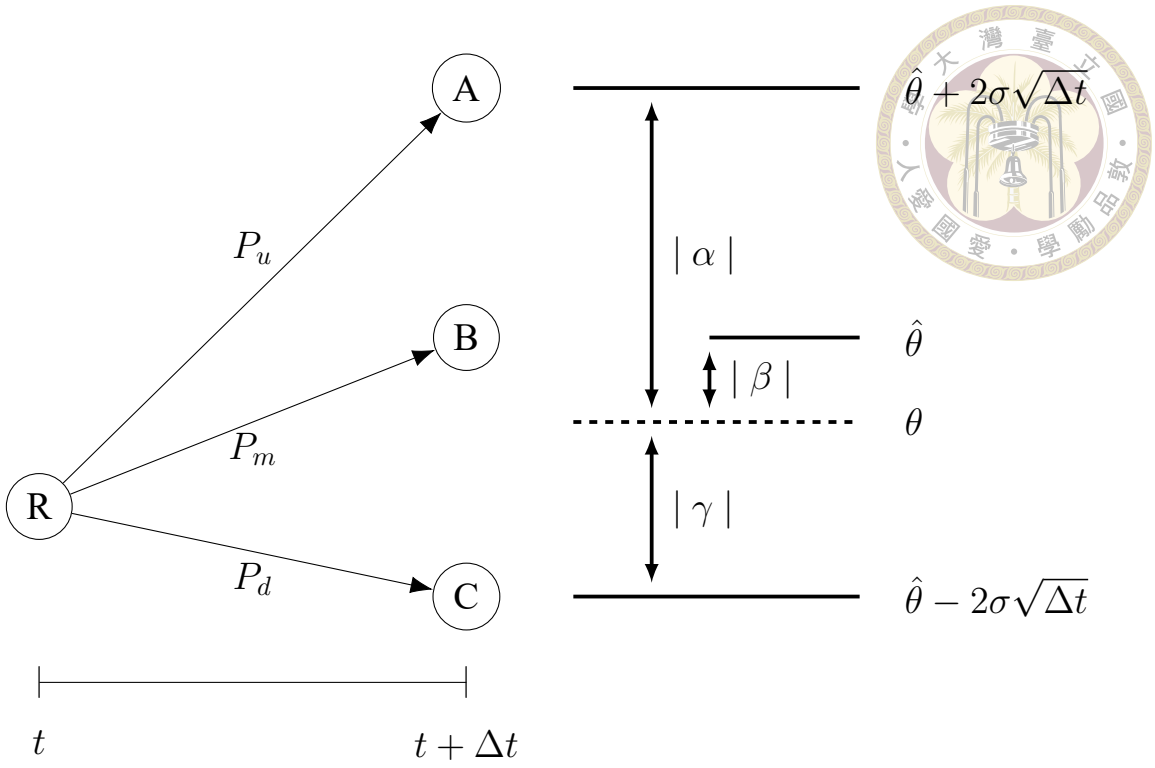

Figure 2.4: The trinomial structure of a BTT.

cess (2.3). Equations (2.10) and (2.11) match the mean and variance of the underlying model. Equation (2.12) makes sure they are probabilities when they are also non-negative. By Cramer's rule, $P_u = \Delta_u/\Delta$, $P_m = \Delta_m/\Delta$, and $P_d = \Delta_d/\Delta$, where

$$\Delta \equiv (\beta-\alpha)(\gamma-\beta)(\gamma-\alpha) = -16\left(\sigma\sqrt{\Delta t}\right)^3, \tag{2.13}$$

$$\Delta_u \equiv (\beta\gamma + \text{Var})(\gamma-\beta) = -2\sigma\sqrt{\Delta t}(\beta\gamma+\text{Var}), \tag{2.14}$$

$$\Delta_m \equiv (\alpha\gamma + \text{Var})(\alpha-\gamma) = 4\sigma\sqrt{\Delta t}(\alpha\gamma+\text{Var}), \tag{2.15}$$

$$\Delta_d \equiv (\alpha\beta + \text{Var})(\beta-\alpha) = -2\sigma\sqrt{\Delta t}(\alpha\beta+\text{Var}). \tag{2.16}$$

Appendix 5.5.3 proves the validity of the three probabilities. Note that β determines the actual positions of nodes A, B, and C on the lattice, thus the whole binomial structure by

doi:10.5566/NTU2018XXXXX

extension. From formulas (2.6)–(2.8) and (2.13)–(2.16):

$$P_u = \frac{\left(\beta - \sigma\sqrt{\Delta t}\right)^2}{8\sigma^2\Delta t}, \tag{2.17}$$

$$P_m = \frac{3\sigma^2\Delta t - \beta^2}{4\sigma^2\Delta t}, \tag{2.18}$$

$$P_d = \frac{\left(\beta + \sigma\sqrt{\Delta t}\right)^2}{8\sigma^2\Delta t}. \tag{2.19}$$

Note that P_u, P_m, and P_d are quadratic functions of β, which is a critical property in solving the implied barrier later.

Incidentally, making the middle branch track the expected logarithmic return instead of simply being flat, a standard choice, solves the notorious barrier-too-close problem (see [26]). This problem refers to the need of very large n for trees when the barrier level of a barrier option is very close to the initial stock price in order to maintain accuracy. The experiments will confirm that our algorithms obtain implied barriers and option prices fast and accurately even when the barrier is extremely close to the initial stock price.

doi:10.5566/NTU2018XXXXX

doi:10.5566/NTU2018XXXXX

Chapter 3: Algorithms

This chapter introduces the algorithm for finding the implied barrier and its adaptations. Section 3.1 describes the core algorithm for finding the implied step barrier and its time complexity. Section 3.2 explains how the core algorithm can be applied to barrier-option pricing. It then shows how the core algorithm can be adapted to different types of moving barriers. Finally, we discuss how to adjust the algorithm to deal with time-varying models. Section 3.3 presents the numerical results of the core algorithm and its adaptations.

3.1 The Core Algorithm

Our core algorithm works with a step barrier. We begin by introducing the notations and terminology used in this chapter. A step barrier consists of m barrier levels for contiguous yet disjoint time intervals $(\,t_0, t_0+t_1\,]$, $(\,t_0+t_1, t_0+t_2\,]$, …, $(\,t_0+t_{m-1}, t_0+t_m\,]$. Each barrier level is left-continuous but not right-continuous by this convention. In this chapter, we let t_0 represent the current time, which makes $t_0 = 0$ (see Figure 3.1). The core algorithm works with one BTT per time interval to find the barrier levels b_1, b_2, …, b_m that give rise to the barrier-hitting probabilities p_1, p_2, …, p_m observed at time t_0 (see Figure 3.2). Specifically, p_i denotes the probability of the stock price hitting the barrier

doi:10.5566/NTU2018XXXXX

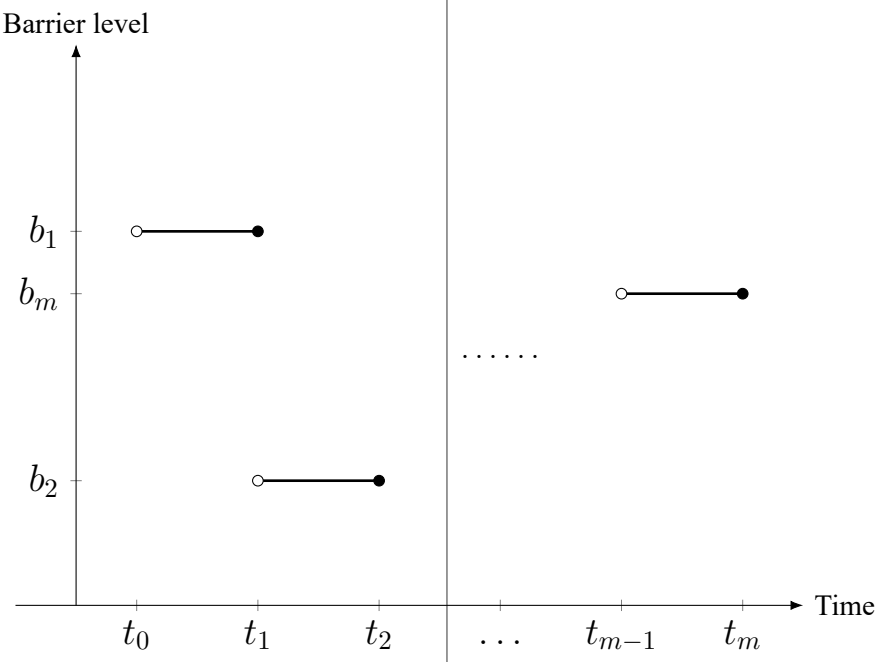

Figure 3.1: A step barrier with m time intervals.

on or before the monitored time point $t_0 + t_i$. We assume $p_1 < p_2 < \cdots < p_m$ to avoid easy-to-handle degenerate cases and add $p_0 = 0$ for convenience.

Assume Δt divides $t_i - t_{i-1}$ for all $1 \leq i \leq m$. This can be enforced by rounding each t_i to the nearest multiple of Δt. Let $n_i \equiv (t_i - t_{i-1})/\Delta t - 1$ denote the number of time steps from time $t_{i-1} + \Delta t$ through time t_i. So there are $n_i + 1$ time steps in time interval $(t_{i-1}, t_i]$, and $t_m - t_0$ is divided into $n = \sum_{i=1}^{m}(n_i + 1)$ time steps. Note that $n_i = O(n/m)$. For brevity, assume all n_is are even.

We adopt the following terms. The survival probability at time t_i, $1 - p_i$, is the probability of the stock price not hitting the barrier between times t_0 and t_i. By the survival probability of a node we mean the probability of that node being reached from the root node at time t_0 without ever hitting the barrier in the process. A node's time-t survival probability denotes that node's survival probability at some future time t.

The core algorithm iterates the following two parts for $1 \leq i \leq m$: (1) Find the

doi:10.5566/NTU2018XXXXX

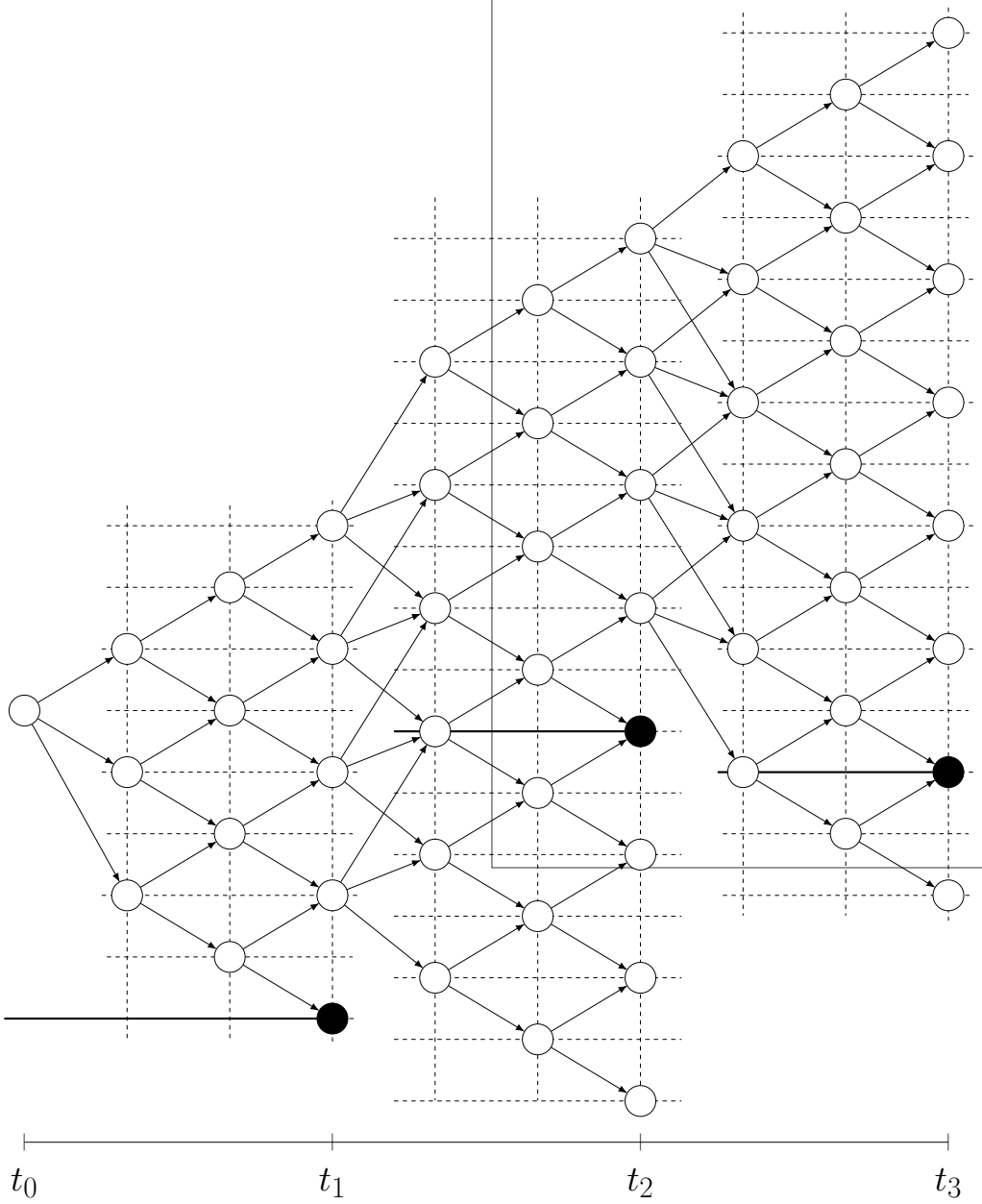

Figure 3.2: A tree with three BTTs. The BTTs cover time intervals $(t_0, t_1]$, $(t_1, t_2]$, and $(t_2, t_3]$.

barrier level b_i for the time interval $(t_{i-1}, t_i]$ that yields $1 - p_i$, the survival probability at time t_i, and (2) propagate the survival probabilities of the nodes above the barrier level b_{i-1} at time t_{i-1} to the nodes above the barrier level b_i at time t_i. The next two Subsections, 3.1.1 and 3.1.2, address these two parts, respectively.

doi:10.5566/NTU2018XXXXX

3.1.1 Finding the Exact Implied Barrier Level

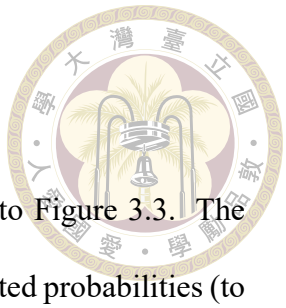

We will describe part (1) of the core algorithm with reference to Figure 3.3. The labels R_0–R_2 and A_0–A_4 there refer to both the nodes and their associated probabilities (to be specified later) for economy of notations. By induction, the survival probabilities of the nodes at time t_{i-1} (nodes R_0–R_2) have been obtained in the previous iteration. Now grow a BTT from those nodes through time t_i. For efficiency's sake, this tree must not actually be built. (In contrast, what we shall call standard algorithms build trees and apply forward induction to propagate the survival probabilities node by node; they are otherwise identical to the core algorithm.) Place the middle branch of each trinomial structure (nodes A_1–A_3) so they all have the same logarithmic return of $\theta - \sigma\sqrt{\Delta t}$. That means $\beta = -\sigma\sqrt{\Delta t}$, $P_u = P_m = 0.5$, and $P_d = 0$ by formulas (2.17)–(2.19). Line up the lattice for the binomial structure with those nodes at time $t_{i-1} + \Delta t$ (nodes A_0–A_4). This positioning of the underlying lattice, thus the binomial structure as well, will be fine-tuned later by adjusting β.

Next, perform a binary search on the tree nodes at time t_i (nodes N_0–N_6) as the barrier levels. It starts with the interval spanning the lowest barrier (node N_0) through the upmost barrier (node N_6). The lowest barrier has no possibility of being hit with $P_d = 0$, while survival is impossible with the upmost barrier. They thus yield survival probabilities 0 and $1 - p_{i-1}$ at time t_i, respectively, which automatically bracket the target $1 - p_i$ as $p_{i-1} < p_i$. The search then picks the middle node at time t_i as barrier and calculates the resulting survival probability at time t_i (to be described in the following paragraphs). It continues with the subinterval whose survival probabilities at time t_i bracket $1 - p_i$ and repeats the halving procedure. Stop when the subinterval narrows down to two adjacent barrier levels,

doi:10.5566/NTU2018XXXXX

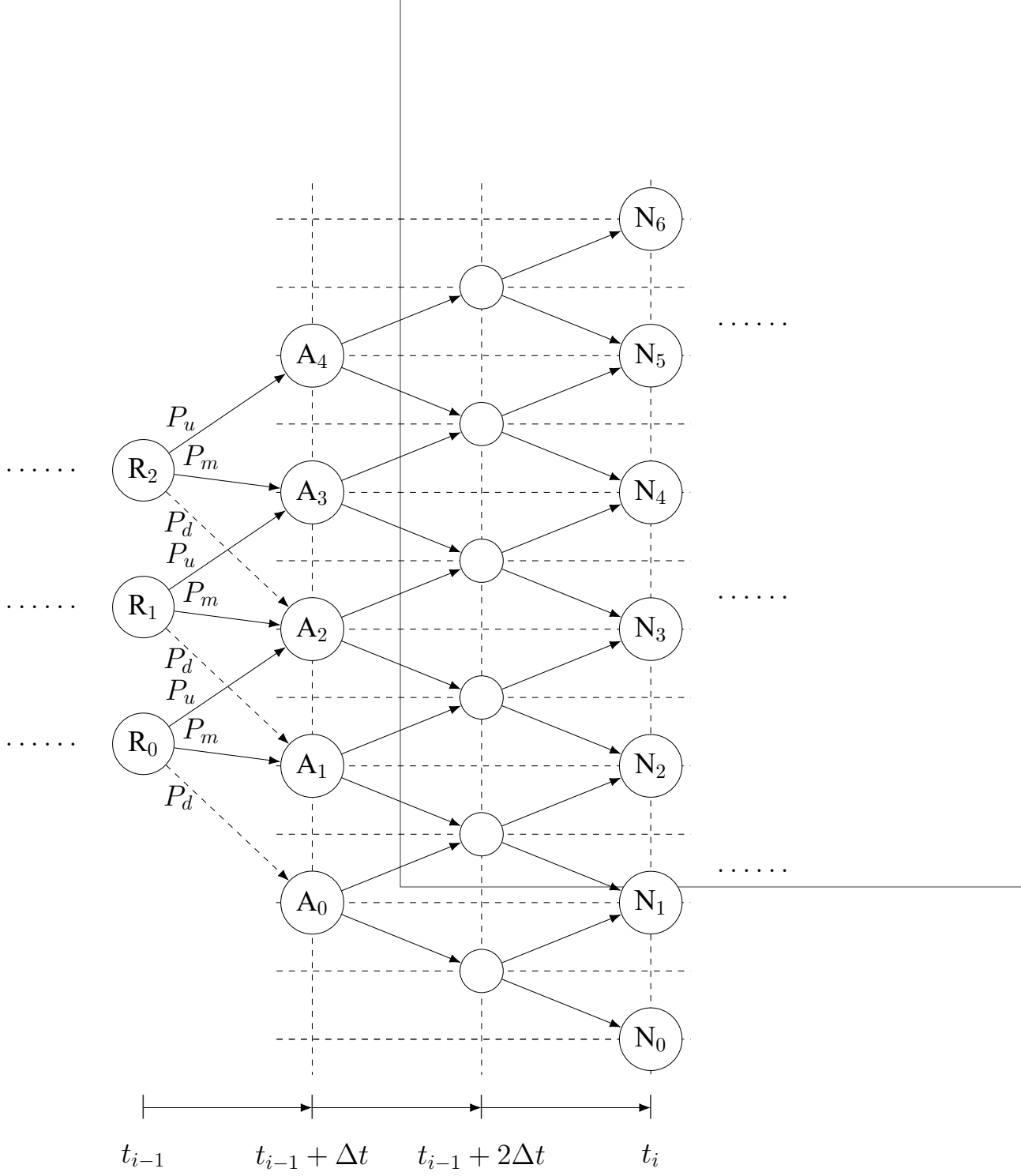

Figure 3.3: The initial BTT with $n_i = 2$. The dashed lines have zero probabilities P_d.

say N_2 and N_3.

We return to obtaining the survival probability at time t_i induced by a selected barrier level. Consider any node above the barrier at time t_{i-1}. Sum the time-t_i survival probabilities of its three successor nodes at time $t_{i-1} + \Delta t$ weighted by the respective branching probabilities P_u, P_m, and P_d, and then multiply this sum by the node's survival probability. Finally, add up such sums to obtain the desired survival probability at time t_i. For

doi:10.5566/NTU2018XXXXX

example, suppose N_0 is the barrier level. The survival probability at time t_i equals

$$\begin{aligned} & (\mathrm{A}_0 P_d + \mathrm{A}_1 P_m + \mathrm{A}_2 P_u)\,\mathrm{R}_0 \\ + \quad & (\mathrm{A}_1 P_d + \mathrm{A}_2 P_m + \mathrm{A}_3 P_u)\,\mathrm{R}_1 \\ + \quad & (\mathrm{A}_2 P_d + \mathrm{A}_3 P_m + \mathrm{A}_4 P_u)\,\mathrm{R}_2, \end{aligned} \tag{3.1}$$

where R_0, R_1, R_2 double as these nodes' survival probabilities, and A_0–A_4 double as these nodes' time-t_i survival probabilities. We next show how to efficiently calculate (i) the time-t_i survival probabilities (like A_0–A_4) and (ii) the survival probability at time t_i (like formula (3.1)).

We start with task (i). Consider any node above the barrier at time $t_{i-1}+\Delta t$. Suppose this node needs to take $2 \le \ell \le n_i$ consecutive down moves to reach the barrier. We call the number of such moves the distance to barrier. Note that ℓ is even because n_i is even. In Figure 2.3, for example, node B needs $\ell = 4$ consecutive down moves to reach the barrier L. Consider paths starting from that node with $n_i - j$ up moves and j down moves that hit the barrier. Their count is $\binom{n_i}{j-\ell}$ by substituting $u = \ell$ and $v = n_i - 2j + \ell$ into formula (2.5). The time-t_i survival probability of the node is

$$B_\ell \quad \equiv \quad \sum_{j=0}^{\frac{n_i+\ell}{2}-1} \binom{n_i}{j} p^{n_i-j}(1-p)^j - \sum_{j=\ell}^{\frac{n_i+\ell}{2}-1} \binom{n_i}{j-\ell} p^{n_i-j}(1-p)^j. \tag{3.2}$$

Set $\mathrm{B}_0 = 0$. Let G_1 and G_2 be the first and second terms in formula (3.2), respectively. The same formula says the time-t_i survival probability of the node immediately below the

doi:10.5566/NTU2018XXXXX

above-mentioned node, whose distance to barrier is $\ell - 2 \geq 0$,

$$B_{\ell-2} \equiv \sum_{j=0}^{\frac{n_i+\ell-2}{2}-1} \binom{n_i}{j} p^{n_i-j}(1-p)^j - \sum_{j=\ell-2}^{\frac{n_i+\ell-2}{2}-1} \binom{n_i}{j-(\ell-2)} p^{n_i-j}(1-p)^j$$

$$= \left[G_1 - \binom{n_i}{\frac{n_i+\ell}{2}-1} p^{\frac{n_i-\ell}{2}+1}(1-p)^{\frac{n_i+\ell}{2}-1}\right] - \left(\frac{p}{1-p}\right)^2 \left[G_2 + \binom{n_i}{\frac{n_i-\ell}{2}} p^{\frac{n_i-\ell}{2}}(1-p)^{\frac{n_i+\ell}{2}}\right]. \quad (3.3)$$

Among the nodes that are positioned above the barrier at time $t_{i-1} + \Delta t$, not more than $n_i/2$ have time-t_i survival probabilities less than 1 because at most that many of them have a distance to barrier not exceeding n_i. The rest, if there are any, need no calculations because their time-t_i survival probabilities equal 1. Reserve $B_\ell = 1$ for them. Start with the node whose distance to barrier is less than, but closest to, n_i. This node's time-t_i survival probability takes $O(n_i)$ time to compute by formula (3.2). Next, apply formula (3.3) iteratively to obtain each of the above-mentioned $O(n_i)$ nodes' time-t_i survival probabilities. Since formula (3.3) takes $O(1)$ time to calculate with G_1 and G_2 available, it takes $O(n_i)$ time to obtain the time-t_i survival probabilities of all the nodes above the barrier at time $t_{i-1} + \Delta t$.

We now describe how task (ii), i.e., the survival probability at time t_i like formula (3.1), can be efficiently calculated from the B_ℓs with translation invariance. We illustrate the idea

doi:10.5566/NTU2018XXXXX

with examples. First, restructure formula (3.1) as

$$\begin{aligned} & (\mathrm{R}_0 P_d)\,\mathrm{A}_0 \\ + \quad & (\mathrm{R}_0 P_m + \mathrm{R}_1 P_d)\,\mathrm{A}_1 \\ + \quad & (\mathrm{R}_0 P_u + \mathrm{R}_1 P_m + \mathrm{R}_2 P_d)\,\mathrm{A}_2 \\ + \quad & (\mathrm{R}_1 P_u + \mathrm{R}_2 P_m)\,\mathrm{A}_3 \\ + \quad & (\mathrm{R}_2 P_u)\,\mathrm{A}_4. \end{aligned} \tag{3.4}$$

Above, A_0, A_1, A_2, A_3, and A_4 equal B_2, B_4, B_6, B_8, and B_{10}, respectively. The probabilities A_0–A_4 change as the barrier level changes. Fortunately, recalculation is unnecessary because nodes with the same distance to barrier have the same time-t_i survival probability by translation invariance. For example, the time-t_i survival probability of node A_2 with N_2 as the new barrier level equals that of node A_0 with N_0 as the barrier level. So if we raise the barrier from N_0 to N_2, the survival probability at time t_i becomes

$$\begin{aligned} & (\mathrm{R}_0 P_u + \mathrm{R}_1 P_m + \mathrm{R}_2 P_d)\,\mathrm{A}_2 \\ + \quad & (\mathrm{R}_1 P_u + \mathrm{R}_2 P_m)\,\mathrm{A}_3 \\ + \quad & (\mathrm{R}_2 P_u)\,\mathrm{A}_4. \end{aligned} \tag{3.5}$$

But now each node A_k being relative to the new level N_2, its time-t_i survival probability will take on that of A_{k-2} when N_0 was the barrier. So the values of A_2, A_3, and A_4 now equal B_2, B_4, and B_6, respectively, instead of the earlier B_6, B_8, and B_{10}. It takes $O(\sum_{j=1}^{i-1} n_j)$ steps to calculate the survival probability at time t_i because formulas (3.4) and (3.5) have as many terms.

We summarize the running time so far. There are at most $1 + \sum_{j=1}^{i}(n_j + 2) = O(n)$

doi:10.5566/NTU2018XXXXX

nodes above the barrier at time t_i. For each node proposed as barrier level, it takes $O(\sum_{j=1}^{i-1} n_j)$ steps to calculate the survival probability at time t_i. With the bisection method, up to $O(\log n)$ barrier levels are considered before the two bracketing nodes are identified. Overall, the algorithm spends $O(\sum_{j=1}^{i-1} n_j \log n)$ time to find the two bracketing nodes.

There are two ways the binary search may end. First, it stops if the survival probability induced by an endpoint of the subinterval as the barrier level matches $1 - p_i$. In this case, the algorithm returns that barrier level. Otherwise, the subinterval is delimited strictly by two adjacent terminal nodes, say N_1 and N_2. This subinterval brackets the desired implied barrier level within a small interval of width $2\sigma\sqrt{\Delta t}$. Still, each remains at best an approximation to b_i.

Surprisingly, the BTT can find the exact b_i that yields the target probability $1 - p_i$ by nudging the underlying lattice with the right amount: It is a simple act of solving a quadratic equation. To begin with, we know b_i must lie between the bracketing nodes (nodes N_2 and N_3). This is because the survival probability at time t_i is a continuous function of β for $-\sigma\sqrt{\Delta t} \le \beta \le \sigma\sqrt{\Delta t}$ by formulas (2.17)–(2.19). It remains to position the barrier level by finding the right β within the interval to yield a survival probability at time t_i equal to $1 - p_i$. Observe that all the trinomial structures share the same β and branching probabilities because they straddle across two lattices with the same interlinear spacing $\sigma\sqrt{\Delta t}$. By our initial choice of $\beta = -\sigma\sqrt{\Delta t}$, nodes A_1, A_2, and A_3 have logarithmic returns of $\theta - 3\sigma\sqrt{\Delta t}$, $\theta - \sigma\sqrt{\Delta t}$, and $\theta + \sigma\sqrt{\Delta t}$ on node R_1, respectively (the branch to node A_1 has zero probability, however). The same holds for the logarithmic returns of nodes A_2, A_3, and A_4 on node R_2, and so on. This implies that the survival probability at time t_i is a linear function of P_u, P_m, and P_d, thus a quadratic function of β by formu-

doi:10.5566/NTU2018XXXXX

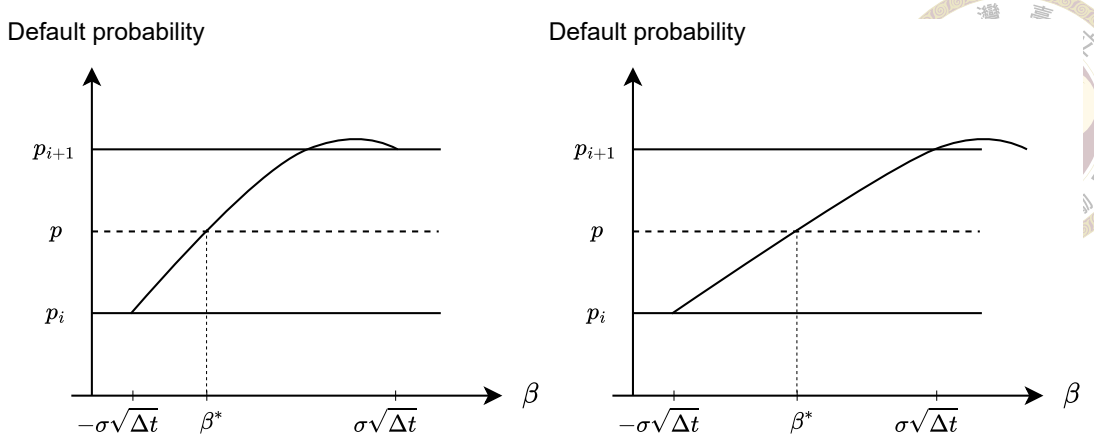

Figure 3.4: The default probability as a concave quadratic function of β. The function's maximum may occur before (the left panel) or after (the right panel) $\sigma\sqrt{\Delta t}$.

las (2.17)–(2.19). It takes $O(n_i)$ time to assemble the three coefficients of the quadratic function. Now solve the $\beta \in [\,-\sigma\sqrt{\Delta t}, \sigma\sqrt{\Delta t}\,]$ that equates the quadratic function with $1 - p_i$. Because the function is concave and brackets $1 - p_i$ at the two endpoints of the subinterval, it has a unique solution β^* within range (2.9) as illustrated in Figure 3.4. (Recall that we started with $\beta = -\sigma\sqrt{\Delta t}$.) The underlying grid will move up by $\beta^* + \sigma\sqrt{\Delta t}$. Finally, the algorithm returns the level of the lower end of the final subinterval (node N_1) as the implied barrier level.

In summary, iteration i of part (1) takes time

$$O\left[n_i + \left(\sum_{j=1}^{i-1} n_j \log n\right) + n_i\right] = O\left(n_i + \sum_{j=1}^{i-1} n_j \log n\right).$$

With m iterations in total, part (1) takes time

$$O\left[\sum_{i=1}^{m}\left(n_i + \sum_{j=1}^{i-1} n_j \log n\right)\right] = O\left[\sum_{i=1}^{m}\left(\frac{n}{m} + \sum_{j=1}^{i-1} \frac{n \log n}{m}\right)\right] = O\left(mn \log n\right).$$

This time bound can be reduced to $O\,[\,mn \log (n/m)\,]$ by recalling that $\mathrm{B}_\ell = 1$ for $\ell > n_i$, which simplifies the overwhelming majority of the terms in formula (3.4). But as m is a constant, this improvement is not pursued further.

doi:10.5566/NTU2018XXXXX

3.1.2 Propagating the Survival Probabilities

Part (2) obtains the survival probability of every node above b_i at time t_i from those above b_{i-1} at time t_{i-1}. We shall accomplish this task efficiently with the combinatorics and FFT.

The first step obtains the survival probabilities of the nodes above b_i at $t_{i-1} + \Delta t$. This is easily done by summing the contributions from the survival probabilities of its predecessor nodes at time t_{i-1} weighted by P_u, P_m, and P_d. For example, the survival probability of node A_2 in Figure 3.3 is

$$\mathrm{R}_0 P_u + \mathrm{R}_1 P_m + \mathrm{R}_2 P_d.$$

Let k_i denote the number of nodes above b_i at time $t_{i-1} + \Delta t$. Name the survival probabilities of these nodes from the top down $q_{k_i-1}, q_{k_i-2}, \ldots, q_0$. Ignore the barrier b_i for the time being. Since the binomial structure has n_i steps, each node at time $t_{i-1} + \Delta t$ will reach those at time t_i with the binomial distribution $B(n_i, p)$. In totality, those k_i nodes will reach $k_i + n_i$ nodes at time t_i. Call the survival probabilities of these nodes $N_{k_i+n_i-1}$, $N_{k_i+n_i-2}$, ..., N_0, again from the top down. They equal, respectively,

$$q_{k_i-1}c_{n_i},\ q_{k_i-1}c_{n_i-1} + q_{k_i-2}c_{n_i},\ q_{k_i-1}c_{n_i-2} + q_{k_i-2}c_{n_i-1} + q_{k_i-3}c_{n_i},\ \ldots,\ q_0 c_0, \tag{3.6}$$

where $c_j \equiv \binom{n_i}{j} p^j (1-p)^{n_i-j}, j = 0, 1, \ldots, n_i$. Clearly, N_j is the coefficient of x^j in

$$\left(q_{k_i-1}x^{k_i-1} + q_{k_i-2}x^{k_i-2} + \cdots + q_0\right)\left(c_{n_i}x^{n_i} + c_{n_i-1}x^{n_i-1} + \cdots + c_0\right) \tag{3.7}$$

for $0 \le j \le k_i + n_i - 1$. This polynomial multiplication can be performed in time

doi:10.5566/NTU2018XXXXX

$O(k_i \log n_i)$ by the FFT (see [23]). This running time simplifies to $O(n \log n_i)$ as $k_i \leq n$.

Now introduce the barrier b_i. The survival probabilities (3.6) need to be lowered to reflect the presence of the barrier. We will calculate the probability of hitting the barrier for each of the $k_i + n_i$ nodes at time t_i and then subtract it from that node's survival probability given in (3.6). We explain the ideas with reference to Figure 3.5. First, reflect those k_i nodes at time $t_{i-1} + \Delta t$ over the barrier to obtain a reflected binomial structure. In Figure 3.5, the reflected binomial structure emanates from nodes A'_0, A'_1, and A'_2, which start with the same survival probabilities as nodes A_0, A_1, and A_2, respectively. Apply the same polynomial multiplication (3.7) to the reflected binomial structure to obtain the probabilities of reaching its nodes at time t_i. By the reflection principle, these probabilities are the desired probabilities if the following adjustment is made before the multiplication (3.7) commences. Consider any path starting from a node above the barrier at time $t_{i-1} + \Delta t$ (one of the nodes A_0–A_2). Let ℓ be this node's distance to barrier. The up moves and down moves in the reflected path are reversed before the x-axis is hit (recall Figure 2.1). That means the survival probability of each of these k_i nodes in the reflected binomial structure (nodes A'_0–A'_2) needs to be multiplied by $[\,(1-p)/p\,]^{\ell}$ before the polynomials are multiplied. The resulting probabilities of the nodes above the barrier at time t_i are then subtracted from the corresponding probabilities in (3.6). This step also costs $O(n \log n_i)$ time with the FFT.

In summary, each iteration of part (2) takes time

$$O\left(n \log n_i + n \log n_i\right) = O\left(n \log n_i\right) = O\left(n \log \frac{n}{m}\right).$$

doi:10.5566/NTU2018XXXXX

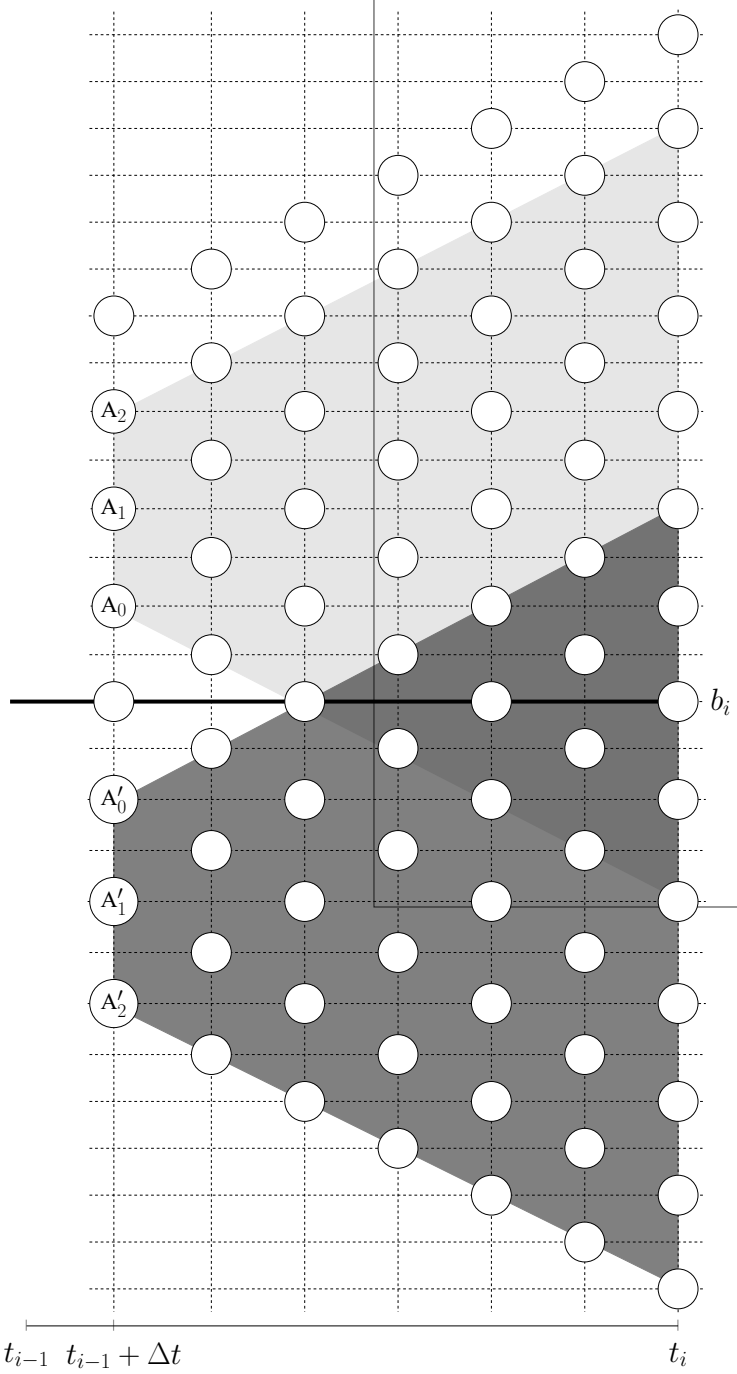

Figure 3.5: The reflected binomial structure. Above, the light gray area contains the binomial structure emanating from the k_i nodes above the barrier at time $t_{i-1} + \Delta t$. Here, $k_i = 3$. The dark gray area contains the binomial structure emanating from these k_i nodes' reflected counterparts. The branches of the binomial structures are not shown.

With m iterations in total, part (2) takes time

$$O\left(mn \log \frac{n}{m}\right).$$

doi:10.5566/NTU2018XXXXX

The pseudo code appears in Algorithm 1.

3.2 Adaptations of the Core Algorithm

Although the core algorithm is to find the implied step barrier, it can be easily specialized to handle other kinds of moving barriers. Moreover, the resulting algorithms become pricing algorithms for options with such barriers after switching to the risk-neutral measure and making minor changes. The above results continue to hold when the growth rate and volatility are time varying.

3.2.1 Barrier Options Pricing

To price step-barrier options, drop part (1) of the core algorithm, which is about finding the implied barrier, thus irrelevant here. Instead, run part (2) to calculate the survival probabilities for the terminal nodes, but under the measure Q, meaning $\mu = r$. Then evaluate the expectation (2.1) by summing the terminal nodes' survival probability-weighted payoffs before discounting the sum, which only takes $O(n)$ time. In total, the running time equals that of part (2) of the core algorithm, $O(mn \log (n/m))$. This $O(n/\log n)$ improvement over the standard algorithm's $O(n^2)$ is dramatic.

3.2.2 Barriers: The Discrete Case

Discrete barriers are monitored at discrete time points. The barrier levels need not be identical. The core algorithm can be simplified to find the implied discrete barrier as follows. Because there is no barrier within time interval (t_{i-1}, t_i) any more, the reflection principle is not needed, and formula (3.2) is reduced to its first term G_1. As a result,

doi:10.5566/NTU2018XXXXX

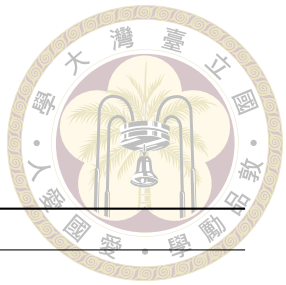

Algorithm 1 The core algorithm

Input: $\mu, \sigma, p_1, p_2, \ldots, p_m, t_0, t_1, t_2, \ldots, t_m, n$.

Output: The implied barrier levels $b_1, b_2, \ldots, b_m$ on the tree that reproduce $p_1, p_2, \ldots, p_m$.

$\Delta t \leftarrow t_m/n$

$t_i \leftarrow \Delta t \times \text{round}(t_i/\Delta t)$ for $i = 1, 2, \ldots, m-1$

for $i \leftarrow 1$ to m **do**

  $n_i \leftarrow [\,(t_i - t_{i-1})/\Delta t\,] - 1$ ▷ Assume n_i is even below for brevity

  Position the initial lattice with $\beta = -\sigma\sqrt{\Delta t}$ ▷ Part (1) starts here

  $\mathrm{B}_\ell \leftarrow \sum_{j=0}^{\frac{n_i+\ell}{2}-1} \binom{n_i}{j} p^{n_i-j}(1-p)^j - \sum_{j=\ell}^{\frac{n_i+\ell}{2}-1} \binom{n_i}{j-\ell} p^{n_i-j}(1-p)^j$ for $\ell = 2, 4, \ldots, n_i$

  $\mathrm{B}_0 \leftarrow 0$ ▷ $\mathrm{B}_\ell = 1$ for $\ell > n_i$ if accessed

  L $\leftarrow$ the lowest node at time t_i reachable from nodes above b_{i-1} at time t_{i-1}

  U $\leftarrow$ the upmost node at time t_i reachable from nodes above b_{i-1} at time t_{i-1}

  $v_\mathrm{L} \leftarrow 1$; $v_\mathrm{U} \leftarrow 0$

  while L and U are not adjacent **do**

    M $\leftarrow$ the median node at time t_i between L and U

    $k_i \leftarrow$ the number of nodes above M at time $t_{i-1} + \Delta t$

    Let $q_{k_i-1}, q_{k_i-2}, \ldots, q_0$ be the survival probabilities of these k_i nodes from the top down

    Let $\ell_{k_i-1}, \ell_{k_i-2}, \ldots, \ell_0$ be these nodes' distances to barrier M

    $v_\mathrm{M} \leftarrow \sum_{j=0}^{k_i-1} q_j B_{\ell_j}$

    if $v_\mathrm{U} < 1 - p_i$ and $v_\mathrm{M} \geq 1 - p_i$ **then**

      L $\leftarrow$ M ; $v_\mathrm{L} \leftarrow v_\mathrm{M}$

    else

      U $\leftarrow$ M ; $v_\mathrm{U} \leftarrow v_\mathrm{M}$

    end if

  end while

  Solve the quadratic function of β for the survival probability that equates $1 - p_i$

  $b_i \leftarrow e^\beta \times$ the stock price of node L

  $k_i \leftarrow$ the number of nodes above b_i at time $t_{i-1} + \Delta t$ ▷ Part (2) starts here

  Let $q_{k_i-1}, q_{k_i-2}, \ldots, q_0$ be the survival probabilities of these k_i nodes from the top down

  Let $\ell_{k_i-1}, \ell_{k_i-2}, \ldots, \ell_0$ be these nodes' distances to barrier b_i

  $c_j \leftarrow \binom{n_i}{j} p^j (1-p)^{n_i-j}$ for $j = 0, 1, \ldots, n_i$

  Let $\sum_{j=0}^{k_i+n_i-1} N_j x^j = \left(\sum_{j=0}^{k_i-1} q_j x^j\right)\left(\sum_{j=0}^{n_i} c_j x^j\right)$

  $s_j \leftarrow [\,(1-p)/p\,]^{\ell_{k_i-1}} q_j$ for $j = 0, 1, \ldots, k_i - 1$

  Let $\sum_{j=0}^{k_i+n_i-1} N'_j x^j = \left(\sum_{j=0}^{k_i-1} s_{k_i-1-j} x^j\right)\left(\sum_{j=0}^{n_i} c_j x^j\right)$

  $N_j \leftarrow N_j - N'_{k_i+\ell_0+j-1}$ for $j = 0, 1, \ldots, n_i - \ell_0$

end for

doi:10.5566/NTU2018XXXXX

formula (3.3) simplifies to

$$B_{\ell-2} \quad \equiv \quad G_1 - \binom{n_i}{\frac{n_i+\ell}{2}-1} p^{\frac{n_i-\ell}{2}+1}(1-p)^{\frac{n_i+\ell}{2}-1}.$$

Part (2) now stops at formula (3.7), omitting the subsequent subtractions to account for the barrier within the time interval. The running time therefore remains the same at $O(mn \log n)$. To price discrete-barrier options, simply follow the idea at the end of Subsection 3.2.1 with the same running time $O(mn \log (n/m))$.

3.2.3 Barriers: The General Case

Suppose the moving barrier alternates between a time interval with a continuously monitored constant barrier level and a time interval with a discretely monitored barrier at the end of it. This setup subsumes the partial and window barriers (see Figure 1.1). To find the implied barrier, simply alternate between the core algorithm and the algorithm in Subsection 3.2.2 with the same running time $O(mn \log n)$. Similarly, such options can be priced in $O(mn \log (n/m))$ time.

For a continuously monitored general moving barrier $b(t)$, the algorithm to find the implied barrier again adopts the core algorithm. But it grows only the trinomial structure of the BTT out of every tree nodes, without the ensuing binomial part (hence $n_i = 0$ for all i). This results in a trinomial tree. The running times are $O(n^2 \log n)$ for finding the implied barrier — because the tree has $O(n^2)$ nodes and the bisection method needs $O(\log n)$ iterations — and $O(n^2)$ for pricing the moving-barrier options.

doi:10.5566/NTU2018XXXXX

3.2.4 Time-Varying Models

So far, our algorithms assumed a constant growth rate μ and volatility σ. When the growth rate $\mu(t)$ and volatility $\sigma(t) > 0$ are time varying, the algorithms for handling continuously monitored moving barriers are the same except for one simple change: The spacing between two vertically adjacent nodes is set to $\sigma'\sqrt{\Delta t}$, where σ' is any upper bound on the volatility function between times t_0 and t_m. As a result, for the nodes residing at time t, formulas (2.6)–(2.8) become

$$\begin{aligned} \alpha &\equiv \beta + \sigma'\sqrt{\Delta t}, \\ \beta &\equiv \hat{\theta} - \theta(t), \\ \gamma &\equiv \beta - \sigma'\sqrt{\Delta t}, \end{aligned}$$

where $\theta(t) \equiv [\,\mu(t) - \sigma^2(t)/2\,]\,\Delta t$. Equation (2.11) becomes

$$P_u\alpha^2 + P_m\beta^2 + P_d\gamma^2 = \sigma^2(t)\,\Delta t.$$

The branching probabilities are guaranteed to be valid for Δt suitably small (see [62]). For pricing, $\theta(t)$ is replaced by $r(t)$, the time-varying risk-free interest rate. The running time is again $O(n^2 \log n)$ for finding the exact implied general moving barrier and $O(n^2)$ for pricing moving-barrier options.

3.3 Numerical Results

This section provides the numerical results on obtaining the exact implied barriers and pricing barrier options for various barrier types. We consider constant barriers, step

doi:10.5566/NTU2018XXXXX

barriers, discrete barriers, and partial barriers. Running times are based on an Amazon EC2 c6g.medium instance. All programs are written in Python using the NumPy package.

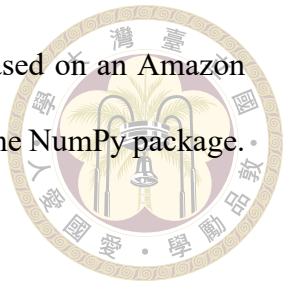

3.3.1 Exact Implied Barriers

The core algorithm produces an exact implied barrier for all n. Although different ns yield different implied barriers, their differences from the true barrier are minuscule even for very small ns in typical cases. The initial stock price is one dollar in this subsection. We first illustrate this with the constant-barrier case, which is treated as a subcase of the step barrier. Given a constant barrier level, the barrier-hitting probability has a well-known formula (see [47]). The solid lines in Figure 3.6 plot the exact implied barriers found by the core algorithm for five different true barrier levels (dotted lines), unknown to the algorithm of course. The exact implied barriers converge quickly and monotonically to the true barrier as n increases. Take the 3rd exhibit for example. The true barrier level is 0.85, and the resulting barrier-hitting probability is 0.424910. The absolute errors start at 0.014 (or 1.647% of the true barrier) for $n = 1$ and decrease smoothly toward zero as n increases. They are less than 0.001 (or 0.133% of the true barrier) for $n \geq 43$. The dashed lines with markers in Figure 3.6 reveal that extrapolating the implied barrier levels from those of n and $2n + 1$ reduces the errors even further (see [7]). Now they start at 0.003 (or within 0.353% of the true barrier) using $n = 1$ and $n = 3$ and never exceed 0.001 (or within 0.118% of the true barrier) when $n \geq 5$.

We make two observations about Figure 3.6. First, in the continuous-time model, the barrier must stay below the current stock price for any non-zero survival probability. But our exact implied barrier might violate that when the true barrier is lower than, but very close to, the current stock price, in which case the barrier-hitting probability is very close

doi:10.5566/NTU2018XXXXX

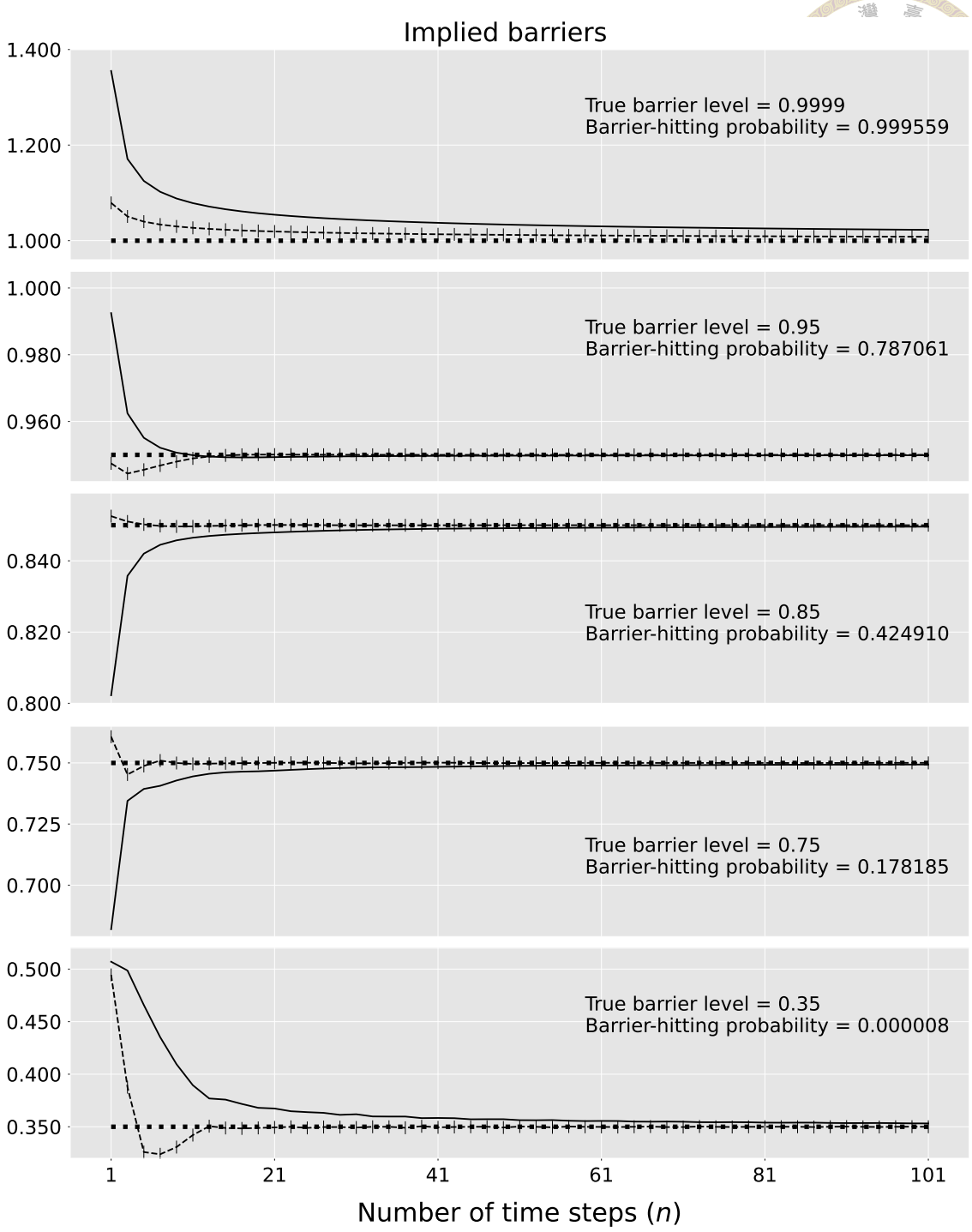

Figure 3.6: The solid lines are the implied barriers from the core algorithm for $n = 1, 3, 5, \ldots, 101$ at five different true barrier levels (dotted lines). The current stock price is 1 dollar, the growth rate is 10%, the volatility is 25%, the horizon is 1 year. The dashed lines with markers are the extrapolated implied barriers using n and $2n + 1$.

to 1. For example, the first exhibit depicts such a barrier-too-close situation to the extreme: The true barrier level 0.9999 is merely 0.0001 below the current stock price 1. The exact implied barrier is found to be 1.355 with a huge relative error of 35.514%. But it quickly

doi:10.5566/NTU2018XXXXX

drops to 1.171 for $n = 3$ and 1.079 after extrapolation using $n = 1$ and $n = 3$. Second, when the true barrier is so low that the resulting barrier-hitting probability is too negligible to encounter in reality, our exact implied barrier may deviate significantly from the true barrier at small ns. For example, the implied barrier is far from the true barrier level 0.35 for small ns in the fifth exhibit, where the barrier-hitting probability is $8.152\,19 \times 10^{-6}$. To address it, one can raise n suitably or apply extrapolation. For example, the relative error is only 1.790% for $n = 51$ and 0.309% after extrapolation using $n = 25$ and $n = 51$. For typical barrier-hitting probabilities such as the middle three exhibits, even $n = 1$ works surprisingly well. We remark that extrapolation will not be applied for the remaining experiments unless explicitly stated.

The literature does not offer true step-barrier option prices for the interesting case of large numbers of barrier levels. We therefore consider $m = 60$ identical month-long barrier levels for a step barrier. The m barrier-hitting probabilities are generated from the well-known formula. Finally, we run the core algorithm, which does not know it is dealt a constant-barrier case, on these probabilities to obtain the exact implied step barrier. The result appears in Figure 3.7. Both the left and right panels plot the exact implied barrier for $n = 180, 780, 1980, 6060$. The true barrier is 0.85 for 5 years in the left panel and 0.9999 for 5 years in the right panel. In both settings, the exact implied barrier converges to the true barrier as n increases.

We next apply the core algorithm to real-world data. The term structures of default probabilities (our cumulative barrier-hitting probabilities p_i) up to 60 months, annual growth rates (μ), and volatilities of asset returns (σ) are provided by the Credit Research Initiative (CRI) of the National University of Singapore.[1] The left exhibit of Figure 3.8

[1] The CRI Dataset, the Credit Research Initiative of the National University of Singapore. We access the dataset on 08-17-2023.

doi:10.5566/NTU2018XXXXX

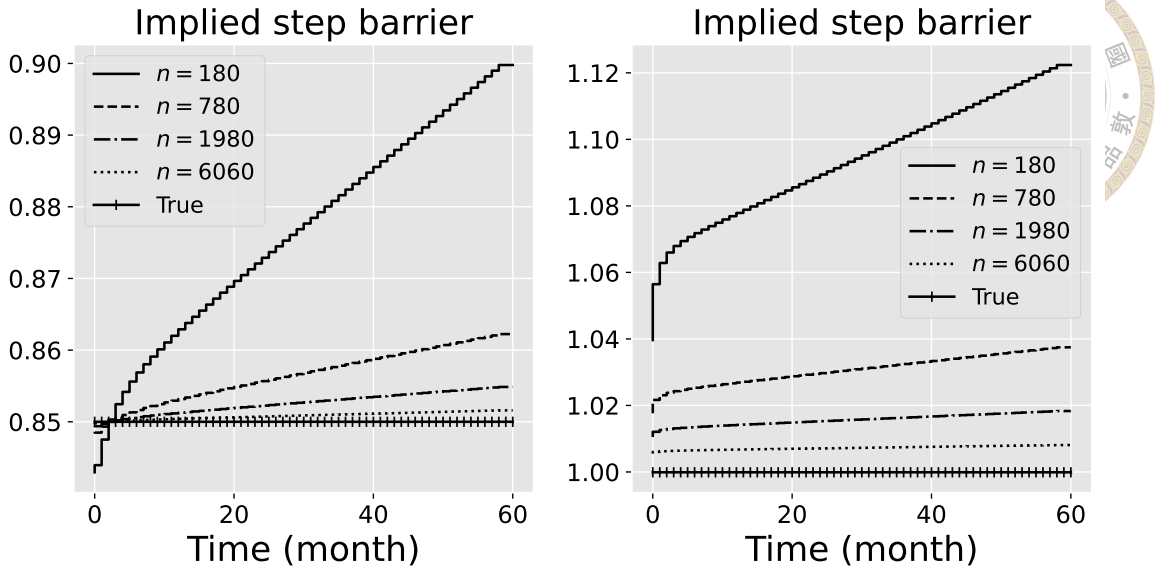

Figure 3.7: The exact implied step barriers by the core algorithm. The parameters are the same as those in Figure 3.6. The true barriers for the left and right exhibits are 0.85 and 0.9999, respectively.

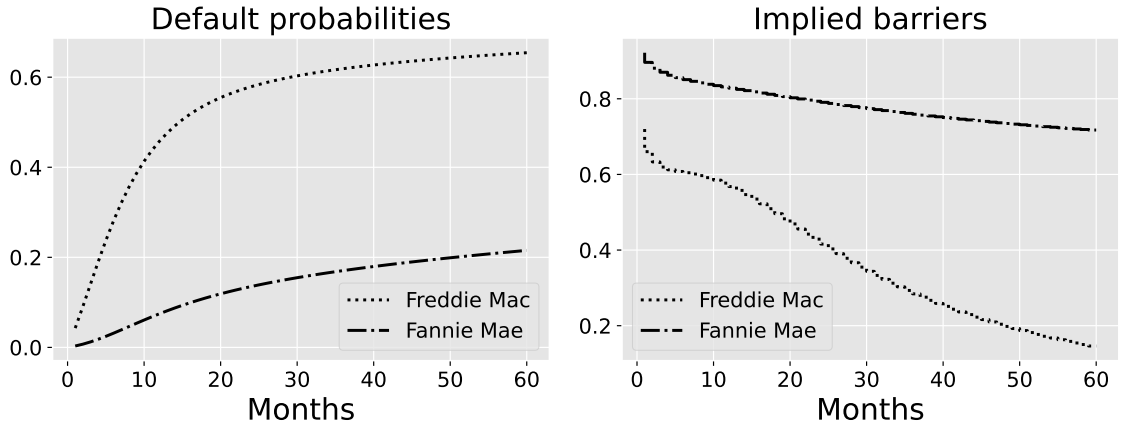

Figure 3.8: Term structures of default probabilities and exact implied step barriers of Freddie Mac and Fannie Mae as of February 2008. The implied step barriers are calculated for $n = 1500$.

plots the default probabilities for Freddie Mac and Fannie Mae as of February 2008. The x-axis represents the number of forward months, and the y-axis denotes the default probability. For example, Freddie Mac (Fannie Mae) has a 40% (8%, respectively) chance of defaulting within the next 10 months. The annual growth rate and volatility of the asset return of Freddie Mac (Fannie Mae) are -1.91% (0.68%, respectively) and 53.72% (9.63%, respectively).

doi:10.5566/NTU2018XXXXX

Table 3.1: Running times (in seconds) of finding the implied barrier of Freddie Mac by the core algorithm and speedups over the standard algorithm.

n	Core algorithm	Standard algorithm	Speedup
780	0.36	3.11	8.59
1500	0.62	7.76	12.55
2340	0.89	15.90	17.87
3180	1.15	26.61	23.19
4500	1.50	49.78	33.10
6060	2.02	82.84	40.92
9060	3.02	179.33	59.30
12060	3.82	307.59	80.51
18060	5.56	663.41	119.29
24060	7.09	1160.80	163.66
30060	9.02	1784.62	197.81
36060	10.92	2592.52	237.39

The right exhibit of Figure 3.8 plots the implied step barriers found by the core algorithm. Both are downward sloping. Table 3.1 tabulates the running times of finding the implied step barrier of Freddie Mac by the core algorithm and the standard algorithm for $780 \leq n \leq 36060$ (in increments of 120). Note that $m = 60$ with the CRI dataset and $n_i = n/m$ for $i = 1, 2, \ldots, 60$. The running times of the core algorithm never exceed 11 seconds. They are also indistinguishable from a linear growth. On the other hand, the standard algorithm takes 3.11 seconds at $n = 780$ and more than two thousands seconds at $n = 36060$. Speedup is defined as the ratio of the running of our core algorithm to that of the standard algorithm (see [50]). The speedups range from 8.59 to 237.39. The core algorithm is obviously much more viable for large portfolios and datasets.

3.3.2 Barrier Options Pricing

Our pricing algorithms are fast and have excellent convergence. Figure 3.9 confirms it with a constant-barrier DOC. As n increases from 201 to 1,401 by increments of 2, the prices converge to 5.9968 given by Merton's (1974) formula. The absolute errors

doi:10.5566/NTU2018XXXXX

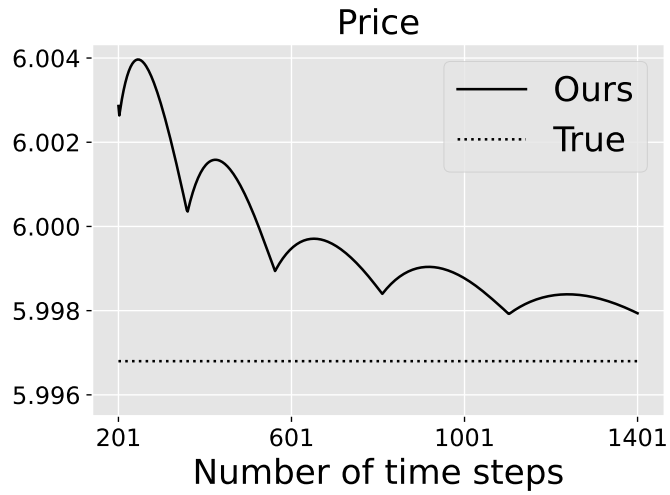

Figure 3.9: Convergence in pricing a constant-barrier DOC by our algorithm. The initial stock price is 95, the strike price is 100, the risk-free interest rate is 10%, the volatility is 25%, the time to maturity is 1 year, and the barrier is 90. The true price is 5.9968 (dotted line).

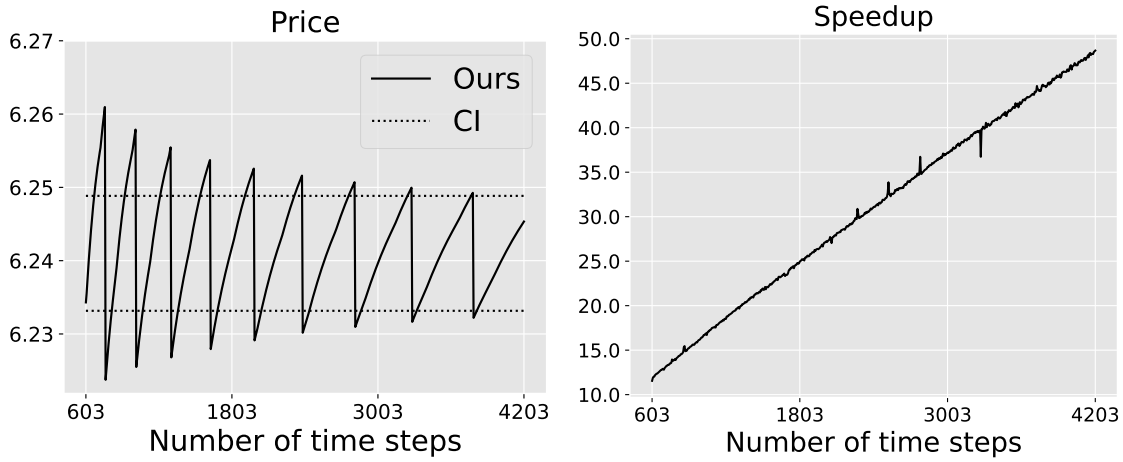

Figure 3.10: Convergence and speedups in pricing a step-barrier DOC by our algorithm. The barrier function is 90 followed by 80 followed by 90 with equal durations. The rest of the parameters are the same as those in Figure 3.9. The left exhibit plots the convergence of our algorithm. The Brownian-bridge method produces a very tight 95% confidence interval (CI) of $[\,6.233, 6.249\,]$ (dotted lines). The right exhibit plots the speedups of our algorithm over the standard algorithm.

are at most 0.001. Figure 3.10 covers the case of a step-barrier DOC. The unbiased and highly efficient Brownian-bridge method of [79] with 10 million paths gives a mean of 6.241 and a standard error of 0.004. Our algorithm's prices never deviate from that by more than 0.02. The speedups over the standard algorithm range from 11.55 to 48.67 for $603 \leq n \leq 4203$ (in increments of 6).

doi:10.5566/NTU2018XXXXX

We next price discrete DOCs at different constant barrier levels with an initial stock price of 100. Our algorithm with extrapolation is compared with the approximation formula of [17]. When $m = 50$ monitoring points, our relative errors are never more than 2.147%. The formula in comparison produces smaller relative errors than ours except when the barrier is 99 (see Table 3.2). Figure 3.11 illustrates the convergence and speedups of our algorithm over the standard algorithm. The speedups trend roughly from 20 to 70 for $5250 \leq n \leq 25250$. Table 3.3 provides the option prices with $m = 5$ and 25. The absolute relative errors of our algorithm stay below 2.170% whereas the formula's reach 4.977% when $m = 25$ and 9.779% when $m = 5$. In general, the formula's performance seems to degrade as the number of monitoring points decreases or as the barrier approaches the initial stock price. Table 3.4 compares the results under different volatilities, times to maturities, and strike prices. As before, the formula's relative errors jump upward when the barrier is close to the initial stock price. Its relative errors also tend to deteriorate when the volatility or the time to maturity increases. In contrast, our algorithm is less sensitive to such parameter changes. Finally, unlike our algorithm, the formula only works for constant barrier levels.

Figure 3.12 illustrates the barrier of a partial-barrier option with a one-year maturity. This barrier starts at the half year and lasts for half a year with a level of 100. The true price is 11.6055 by the formula in [40]. Figure 3.13 depicts the convergence and speedups. Our algorithm converges very fast, and the pricing errors are at most 0.0004. The speedups over the standard algorithm range from 7.05 to 25.86 for $402 \leq n \leq 2802$ (in increments of 4).

doi:10.5566/NTU2018XXXXX

Table 3.2: Comparison of discrete DOC prices with $m = 50$ monitoring points. The initial stock price is 100, the strike price is 100, the risk-free interest rate is 10%, the volatility is 30%, the time to maturity is 0.2 year, and the barrier levels are the same at all the 50 equally spaced monitoring points, which approximates daily monitoring. The 2nd, 4th, and 5th columns are from Table 2.1 of [17]. The 3rd column extrapolates the prices by our algorithm using $n = 12550$ and $n = 25050$.

Barrier level	(a) Broadie et al. (1997)	(b) Our algorithm with extrapolation	True	Relative error (%)	
				(a)	(b)
91	5.977	5.969	5.977	0.000	−0.133
92	5.810	5.799	5.810	0.000	−0.195
93	5.585	5.569	5.584	0.018	−0.262
94	5.288	5.268	5.288	0.000	−0.372
95	4.907	4.882	4.907	0.000	−0.519
96	4.428	4.395	4.427	0.023	−0.728
97	3.836	3.795	3.834	0.052	−1.025
98	3.121	3.080	3.126	−0.160	−1.466
99	2.271	2.287	2.337	−2.824	−2.147

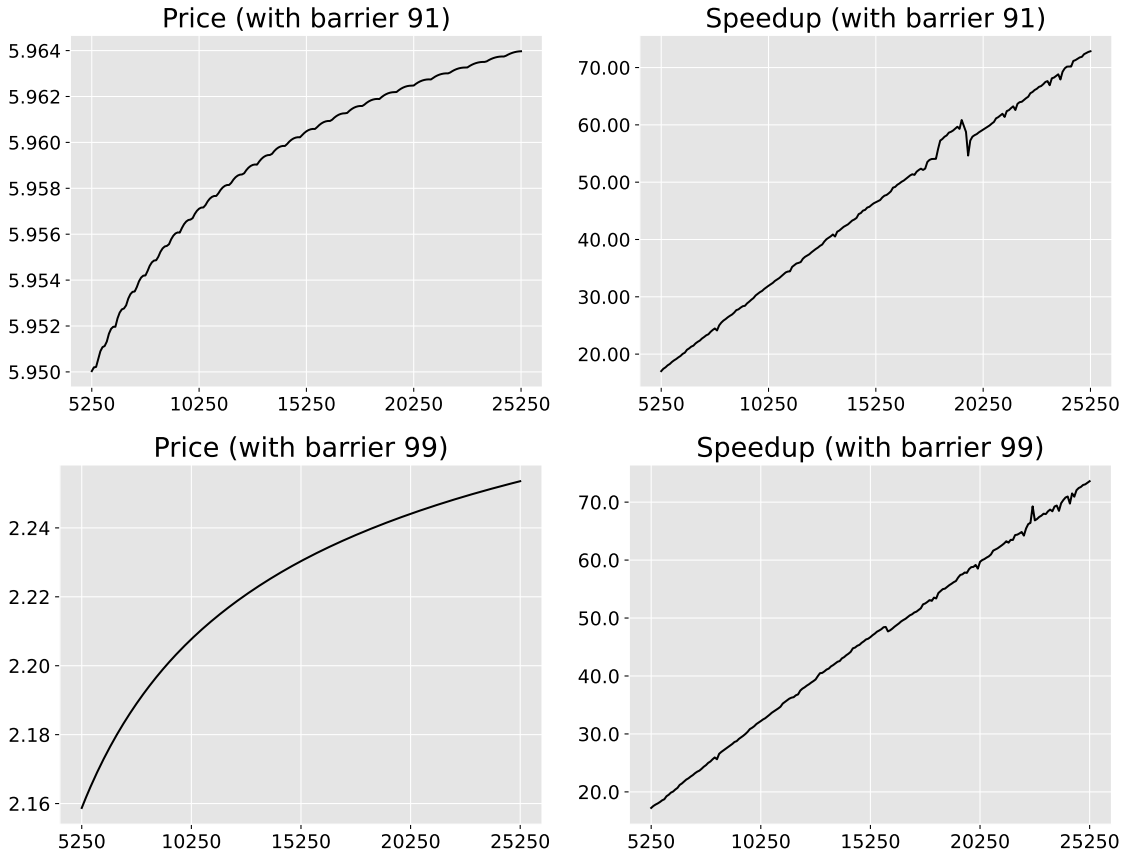

Figure 3.11: Convergence and speedups in pricing discrete DOCs by our algorithm. The parameters are the same as those in Table 3.2. The left exhibits show the convergence of our algorithm. The right exhibits plot the speedups of our algorithm over the standard algorithm. The x-axes denote the number of time steps.

doi:10.5566/NTU2018XXXXX

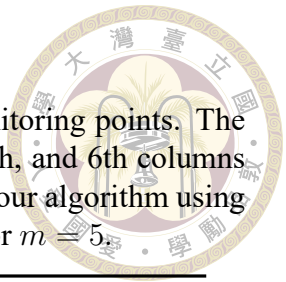

Table 3.3: Comparison of discrete DOC prices with $m = 5,\ 25$ monitoring points. The parameters are the same as those in Table 3.2 except m. The 3nd, 5th, and 6th columns are from Table 2.2 of [17]. The 4th column extrapolates the prices by our algorithm using $n = 6275$ and $n = 12525$ for $m = 25$, and $n = 1255$ and $n = 2505$ for $m = 5$.

m	Barrier level	(a) Broadie et al. (1997)	(b) Our algorithm with extrapolation	True	Relative error (%)	
					(a)	(b)
25	91	6.033	6.022	6.032	0.017	−0.161
	93	5.688	5.669	5.688	0.000	−0.337
	95	5.084	5.049	5.081	0.059	−0.624
	97	4.113	4.067	4.116	−0.073	−1.202
	99	2.673	2.752	2.813	−4.977	−2.170
5	91	6.194	6.175	6.187	0.113	−0.187
	93	6.004	5.977	6.000	0.067	−0.385
	95	5.646	5.633	5.671	−0.441	−0.672
	97	5.028	5.111	5.167	−2.690	−1.080
	99	4.050	4.469	4.489	−9.779	−0.435

Table 3.4: Comparison of discrete DOC prices under different volatilities, times to maturities, and strike prices. The parameters are the same as in Table 3.2 except that Panel A raises the volatility to 60%, Panel B raises the time to maturity to 2 years, and Panel C raises the strike price to 110. The 3rd, 5th, and 6th columns are from Table 2.3 of [17]. The 4th column extrapolates the prices by our algorithm with $n = 12550$ and $n = 25050$.

Panel	Barrier level	(a) Broadie et al. (1997)	(b) Our algorithm with extrapolation	True	Relative error (%)	
					(a)	(b)
A	91	8.573	8.521	8.572	0.012	−0.596
	93	7.566	7.499	7.563	0.040	−0.845
	95	6.346	6.266	6.344	0.032	−1.234
	97	4.900	4.853	4.941	−0.830	−1.771
	99	3.219	3.286	3.475	−7.367	−2.549
B	91	16.446	16.275	16.436	0.061	−0.978
	93	14.534	14.354	14.537	0.021	−1.258
	95	12.371	12.250	12.451	-0.643	−1.617
	97	9.945	10.043	10.254	−3.013	−2.061
	99	7.243	7.950	8.061	−10.148	−1.377
C	91	2.433	2.431	2.433	0.000	−0.078
	93	2.336	2.332	2.336	0.000	−0.158
	95	2.136	2.127	2.135	0.047	−0.358
	97	1.757	1.741	1.756	0.057	−0.864
	99	1.105	1.114	1.136	−2.729	−1.910

doi:10.5566/NTU2018XXXXX

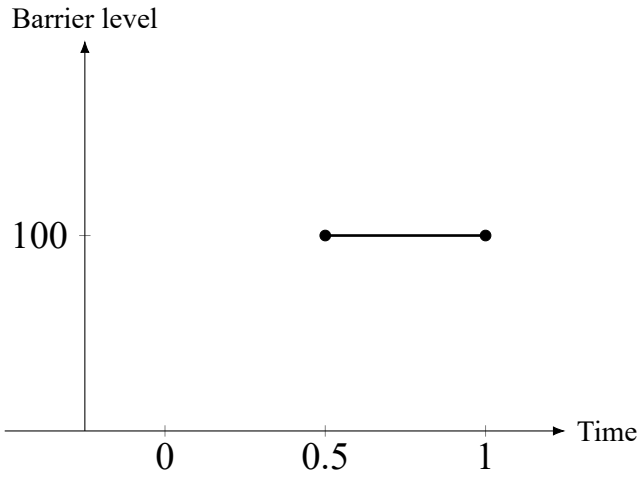

Figure 3.12: A partial barrier.

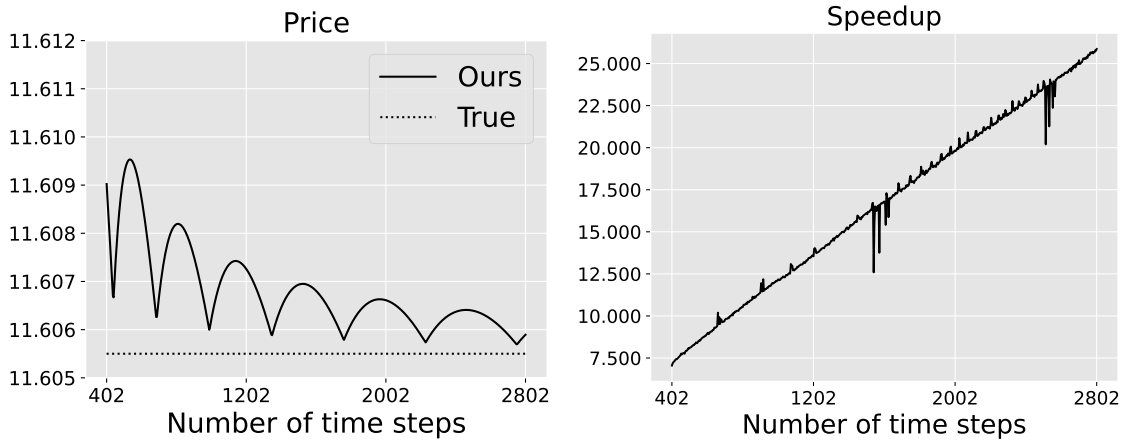

Figure 3.13: Convergence and speedups in pricing a partial-barrier DOC by our algorithm. The initial stock price is 105, the strike price is 110, the interest rate is 10%, the volatility is 25%, and the time to maturity is 1 year. Its barrier appears in Figure 3.12. The left exhibit shows the convergence of our algorithm. The true price is 11.6055 (dotted line). The right exhibit plots the speedups of our algorithm over the standard algorithm.

doi:10.5566/NTU2018XXXXX

doi:10.5566/NTU2018XXXXX

Chapter 4: Convergence Rates

This chapter provides the mathematical proof and the numerical results for the linear convergence rate of the implied barrier from the core algorithm. Section 4.1 proves that the default probability as calculated on the n-step BTT converges to the continuous-time limit at a rate of $O(n^{-1})$. Section 4.2 proves that, in the constant-barrier case, the implied barrier level converges to the true barrier level at a rate of $O(n^{-1})$. Section 4.3 presents the corresponding numerical results. We also show the numerical results of the step-barrier case, which suggest a linear convergence rate as well.

4.1 Linear Convergence of the Default Probability

For logarithmic stock price x (which may depend on n) and time t, let $C^{\mathrm{BS}}(x,t)$ denote the DODC's expected payoff under the BS model and $C_n^{\mathrm{BTT}}(x,t)$ the DODC's expected payoff by the n-step BTT. Barrier is ignored in the notations for brevity. The convergence rate of the DODC's expected payoff by the CRR tree when the barrier passes through a terminal node is covered by the next result, implicit in Lin and Palmer's proof of their Theorem 1.2 (1)(b) [59].

Theorem 1 ([59]). *The expected payoff C_n^{CRR} of a DODC in the n-step CRR tree with initial stock price S_n, strike price and barrier level equal to H_n, which is a node on the*

doi:10.5566/NTU2018XXXXX

grid, and maturity T_n satisfies $C_n^{\text{CRR}} = C^{\text{BS}} + O(n^{-1})$, where C^{BS} is the expected payoff of the same DODC under the BS model, provided that S_n/H_n is bounded and $T_n \to T > 0$.

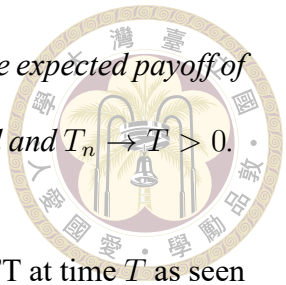

Let P_{A}, P_{B}, and P_{C} be the survival probabilities on the n-step BTT at time T as seen from the root node R's three successor nodes A, B, and C, respectively (recall Figure 2.3). By equations (2.17)–(2.19),

$$C_n^{\text{BTT}}(s_{\text{R}}, 0) = P_u P_{\text{A}} + P_m P_{\text{B}} + P_d P_{\text{C}} \tag{4.1}$$

$$= \frac{P_{\text{A}} - 2P_{\text{B}} + P_{\text{C}}}{8\sigma^2 \Delta t}\beta^2 + \frac{-P_{\text{A}} + P_{\text{C}}}{4\sigma\sqrt{\Delta t}}\beta + \frac{P_{\text{A}} + 6P_{\text{B}} + P_{\text{C}}}{8} \tag{4.2}$$

after simplification. Note that P_{A}, P_{B}, and P_{C} are independent of β because (1) the transition probabilities of the CRR tree are and (2) the number of grid points between nodes A, B, C, and the barrier, respectively, remain constant. Recall that s_z stands for the logarithmic stock price of node z. Define

$$\begin{aligned} C_x^{\text{BS}} &\equiv \frac{\partial C^{\text{BS}}(s_{\text{R}}, 0)}{\partial x}, \\ C_t^{\text{BS}} &\equiv \frac{\partial C^{\text{BS}}(s_{\text{R}}, 0)}{\partial t}, \\ C_{xx}^{\text{BS}} &\equiv \frac{\partial^2 C^{\text{BS}}(s_{\text{R}}, 0)}{\partial x^2}, \end{aligned}$$

and note that

$$\begin{aligned} s_{\text{A}} &= s_{\text{R}} + \alpha + \theta, \\ s_{\text{B}} &= s_{\text{R}} + \beta + \theta, \\ s_{\text{C}} &= s_{\text{R}} + \gamma + \theta \end{aligned}$$

doi:10.5566/NTU2018XXXXX

by equations (2.6)-(2.8). Thus

$$\begin{aligned} P_{\mathrm{A}} &= C^{\mathrm{BS}}\left(s_{\mathrm{A}}, \Delta t\right) + O(\Delta t) \\ &= C^{\mathrm{BS}}\left(s_{\mathrm{R}}, 0\right) + C_x^{\mathrm{BS}}\left(s_{\mathrm{A}} - s_{\mathrm{R}}\right) + C_t^{\mathrm{BS}}\Delta t + \frac{C_{xx}^{\mathrm{BS}}\left(s_{\mathrm{A}} - s_{\mathrm{R}}\right)^2}{2} + O(\Delta t) \\ &= C^{\mathrm{BS}}\left(s_{\mathrm{R}}, 0\right) + C_x^{\mathrm{BS}}(\alpha + \theta) + C_t^{\mathrm{BS}}\,\Delta t + \frac{C_{xx}^{\mathrm{BS}}\left(\alpha + \theta\right)^2}{2} + O(\Delta t) \quad (4.3) \end{aligned}$$

by Theorem 1 (recall that the survival probability equals the expected payoff of the DODC) and the Taylor expansion around $(s_{\mathrm{R}}, 0)$. Similarly,

$$P_{\mathrm{B}} = C^{\mathrm{BS}}\left(s_{\mathrm{R}}, 0\right) + C_x^{\mathrm{BS}}(\beta + \theta) + C_t^{\mathrm{BS}}\,\Delta t + \frac{C_{xx}^{\mathrm{BS}}\left(\beta + \theta\right)^2}{2} + O(\Delta t), \quad (4.4)$$

$$P_{\mathrm{C}} = C^{\mathrm{BS}}\left(s_{\mathrm{R}}, 0\right) + C_x^{\mathrm{BS}}(\gamma + \theta) + C_t^{\mathrm{BS}}\,\Delta t + \frac{C_{xx}^{\mathrm{BS}}\left(\gamma + \theta\right)^2}{2} + O(\Delta t). \quad (4.5)$$

Finally, equation (4.1) with the help of equations (2.10)–(2.12) and (4.3)–(4.5) reduces to

$$\begin{aligned} C_n^{\mathrm{BTT}}\left(s_{\mathrm{R}}, 0\right) &= C^{\mathrm{BS}}(s_{\mathrm{R}}, 0) + \theta C_x^{\mathrm{BS}} + C_t^{\mathrm{BS}}\Delta t + \frac{1}{2}\,C_{xx}^{\mathrm{BS}}\left(\theta^2 + \sigma^2\Delta t\right) + O(\Delta t) \\ &= C^{\mathrm{BS}}(s_{\mathrm{R}}, 0) + O(\Delta t) \end{aligned}$$

as $\theta = O(\Delta t)$. We have proved that $C_n^{\mathrm{BTT}}(s_{\mathrm{R}}, 0) - C^{\mathrm{BS}}(s_{\mathrm{R}}, 0) = O(n^{-1})$ as $\Delta t = O(n^{-1})$. As default probability equals one minus the DODC's expected payoff, we have the first main theorem below.

Theorem 2. *The default probability as calculated on the n-step BTT converges to the continuous-time limit at a rate of $O(n^{-1})$.*

4.2 Linear Convergence of the Implied Barrier

The following simple lemma will be useful later.

doi:10.5566/NTU2018XXXXX

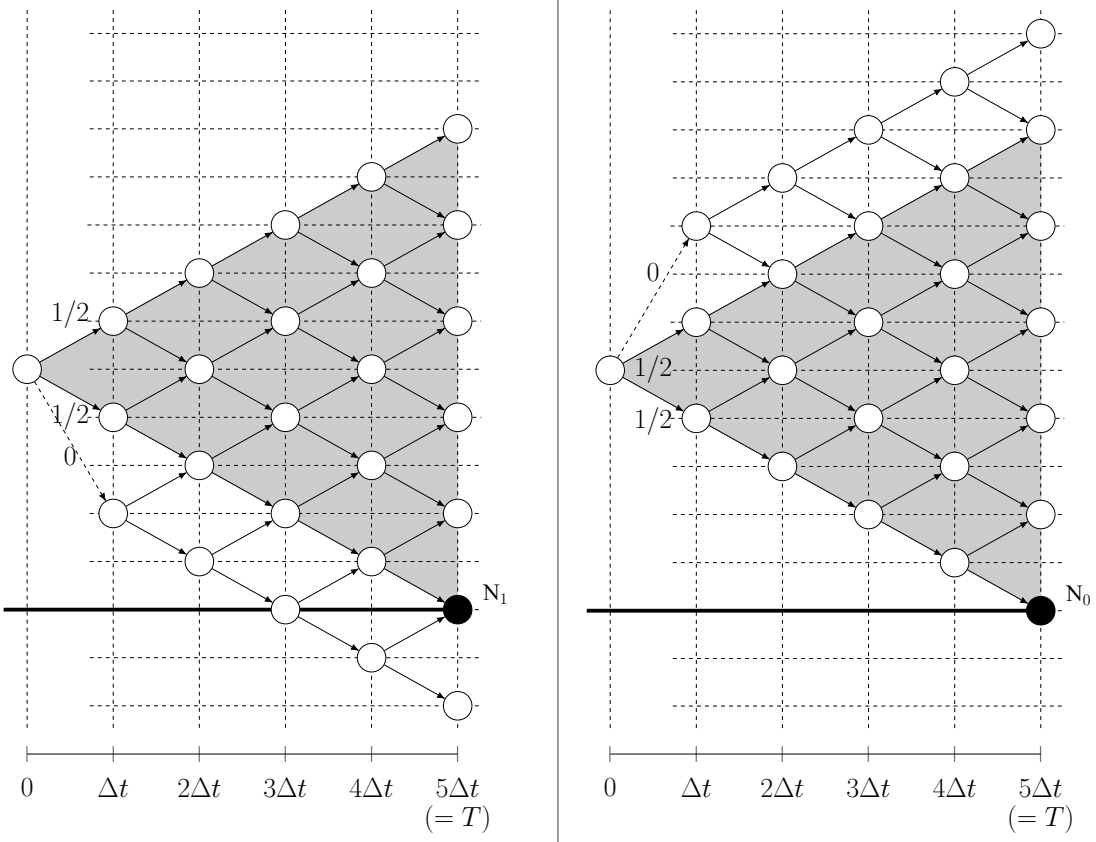

Figure 4.1: Two identical BTTs: $\beta = -\sigma\sqrt{\Delta t}$ (left) and $\beta = \sigma\sqrt{\Delta t}$ (right). The thick black lines indicate the barriers.

Lemma 1. *Label a BTT's terminal nodes at T from bottom to top as N_0, N_1, ..., N_{n+1}. Consider two BTTs: one with $\beta = -\sigma\sqrt{\Delta t}$ and the barrier level is aligned with the terminal node N_k; and another with $\beta = \sigma\sqrt{\Delta t}$ and the barrier level is aligned with N_{k-1}. The probabilities of hitting the barrier are identical.*

Proof. With $\beta = -\sigma\sqrt{\Delta t}$, the transition probabilities are 0.5, 0.5, and 0; with $\beta = \sigma\sqrt{\Delta t}$, the transition probabilities are 0, 0.5, and 0.5. So seen from the root node, the two BTTs are identical when their barrier levels are as specified (see Figure 4.1). □

doi:10.5566/NTU2018XXXXX

The following identities are clear from equations (2.6)–(2.8):

$$\alpha - \gamma = 4\sigma\sqrt{\Delta t}, \tag{4.6}$$

$$\alpha - 2\beta + \gamma = 0, \tag{4.7}$$

$$\alpha^2 - 2\beta^2 + \gamma^2 = 8\sigma^2\Delta t. \tag{4.8}$$

Equation (4.2) with the help of equations (2.6)–(2.8) and (4.3)–(4.8) becomes

$$\begin{aligned} & C_n^{\mathrm{BTT}}(s_{\mathrm{R}}, 0) \\ = \; & \frac{C_{xx}^{\mathrm{BS}}\sigma^2\Delta t + O(\Delta t)}{2\sigma^2\Delta t}\,\beta^2 - \frac{\sigma\sqrt{\Delta t}\left(C_x^{\mathrm{BS}} + C_{xx}^{\mathrm{BS}}\hat{\theta}\right) + O(\Delta t)}{\sigma\sqrt{\Delta t}}\,\beta + \frac{P_{\mathrm{A}} + 6P_{\mathrm{B}} + P_{\mathrm{C}}}{8}. \end{aligned} \tag{4.9}$$

Lemma 2. *The expected payoff of a DODC by the BTT is a quadratic function of β. Furthermore, the coefficient of β^2 and β are $O(1)$, and the β term dominates the β^2 term in magnitude.*

Proof. The expected payoff is quadratic in β by equation (4.2). The coefficients of β^2 and β equal $C_{xx}^{\mathrm{BS}}/2 + O(1)$ and $-C_x^{\mathrm{BS}} - C_{xx}^{\mathrm{BS}}\hat{\theta} + O(\sqrt{\Delta t})$, respectively, by equation (4.9). Both coefficients are $O(1)$ because $\hat{\theta} = O(\sqrt{\Delta t})$ and C_x^{BS} and C_{xx}^{BS} are bounded. Furthermore, the coefficient of β approaches $-C_x^{\mathrm{BS}}$, which is negative and bounded away from zero. The β term dominates the β^2 term in magnitude because $\beta^2 \ll \beta$ for $\beta = O(\sqrt{\Delta t})$. □

Let Q_k be the DODC's expected payoff by the n-step BTT with $\beta = -\sigma\sqrt{\Delta t}$ when terminal node N_k is the barrier level (recall Figure 3.3). Note that $Q_k = 1 - p_k$ and $Q_0 > Q_1 > \cdots$ until the expected payoff reaches zero, where it stays. We are now in a position to prove the main result: The exact implied barrier level differs from the true

doi:10.5566/NTU2018XXXXX

barrier level by $O(n^{-1})$.

Theorem 3. *The exact implied barrier level by the n-step BTT differs from the true barrier level by $O(n^{-1})$.*

Proof. Let p be the default probability. Denote the logarithmic value of the exact implied barrier level by b_n^{imp} and the true logarithmic barrier level by b^{true}, respectively. Note that b^{true} is a constant and below the initial stock price by our convention. Although the goal is $e^{b_n^{\text{imp}}} - e^{b^{\text{true}}} = O(n^{-1})$, it suffices to prove $b_n^{\text{imp}} - b^{\text{true}} = O(n^{-1})$ because, then,

$$e^{b_n^{\text{imp}}} - e^{b^{\text{true}}} \;=\; e^{b_n^{\text{imp}}} \left(1 - e^{b^{\text{true}} - b_n^{\text{imp}}}\right) \;\approx\; e^{b_n^{\text{imp}}} \left(b_n^{\text{imp}} - b^{\text{true}}\right),$$

which converges to zero at a speed of n^{-1}.

The DODC's expected payoff q_n^{imp} induced by b_n^{imp} on the n-step BTT equals $1 - p$ as b_n^{imp} is exact. Assume the algorithm for the implied barrier ends with $\beta = \beta'$. Let q^{true} denote the DODC's expected payoff induced by b^{true} on the n-step BTT which ends with $\beta = \beta''$. Without loss of generality, assume $q_n^{\text{imp}} \geq q^{\text{true}}$; the argument is symmetric if $q_n^{\text{imp}} \leq q^{\text{true}}$. Recall that the default probability equals one minus the DODC's expected payoff. Theorem 2 says

$$q_n^{\text{imp}} - q^{\text{true}} \;=\; O\left(n^{-1}\right). \tag{4.10}$$

Let

$$\begin{aligned} Q_{i+1} \;&\leq\; q_n^{\text{imp}} \;<\; Q_i, \\ Q_{j+1} \;&\leq\; q^{\text{true}} \;<\; Q_j. \end{aligned}$$

Because $q_n^{\text{imp}} \geq q^{\text{true}}$, there are three cases to consider: (1) $i = j$, (2) $i + 1 = j$, and (3)

doi:10.5566/NTU2018XXXXX

$i+1<j$.

For case (1),

$$b^{\text{true}} - b_n^{\text{imp}} \;=\; \beta'' - \beta'$$

(see Figure 4.2). Therefore

$$\left| b_n^{\text{imp}} - b^{\text{true}} \right| \;=\; O\left(q_n^{\text{imp}} - q^{\text{true}}\right) \;=\; O\left(n^{-1}\right),$$

as desired, by equation (4.10) and Lemma 2. For case (2),

$$Q_{i+2} \;\leq\; q^{\text{true}} \;<\; Q_{i+1} \;\leq\; q_n^{\text{imp}} \;<\; Q_i;$$

hence it is necessary that

$$q_n^{\text{imp}} - Q_{i+1} \;=\; O\left(n^{-1}\right),$$

$$Q_{i+1} - q^{\text{true}} \;=\; O\left(n^{-1}\right)$$

by equation (4.10) (see Figure 4.3). Apply the same argument as in case (1) to obtain, separately,

$$\left| b_n^{\text{imp}} - \mathrm{N}_{i+1} \right| \;=\; O\left(q_n^{\text{imp}} - Q_{i+1}\right) \;=\; O\left(n^{-1}\right),$$

$$\left| b^{\text{true}} - \mathrm{N}_{i+1} \right| \;=\; O\left(q^{\text{true}} - Q_{i+1}\right) \;=\; O\left(n^{-1}\right).$$

Finally,

$$\left| b_n^{\text{imp}} - b^{\text{true}} \right| \;\leq\; \left| b_n^{\text{imp}} - \mathrm{N}_{i+1} \right| + \left| \mathrm{N}_{i+1} - b^{\text{true}} \right| \;=\; O\left(n^{-1}\right),$$

as desired. For case (3),

$$q^{\text{true}} \;<\; Q_j \;<\; Q_{i+1} \leq\; q_n^{\text{imp}}.$$

doi:10.5566/NTU2018XXXXX

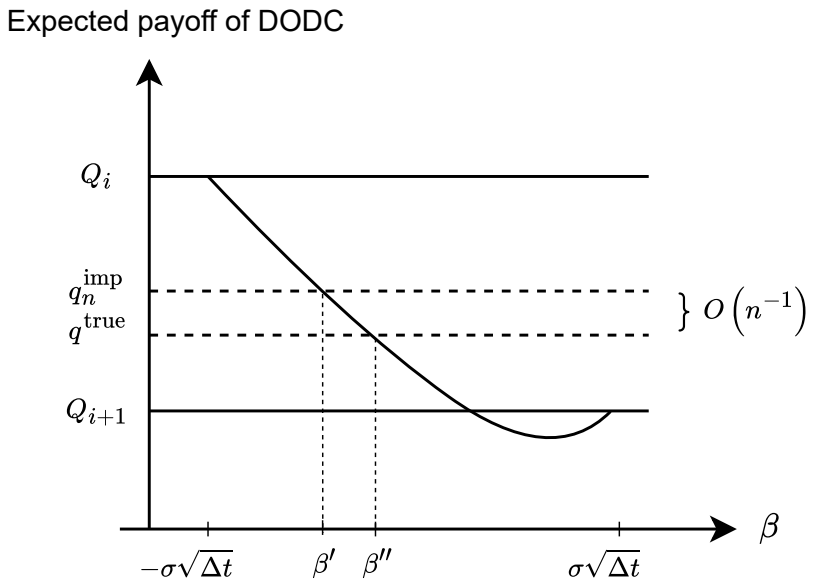

Figure 4.2: Relations among the six quantities Q_i, Q_{i+1}, q_n^{imp}, q^{true}, β' and β'' for case (1).

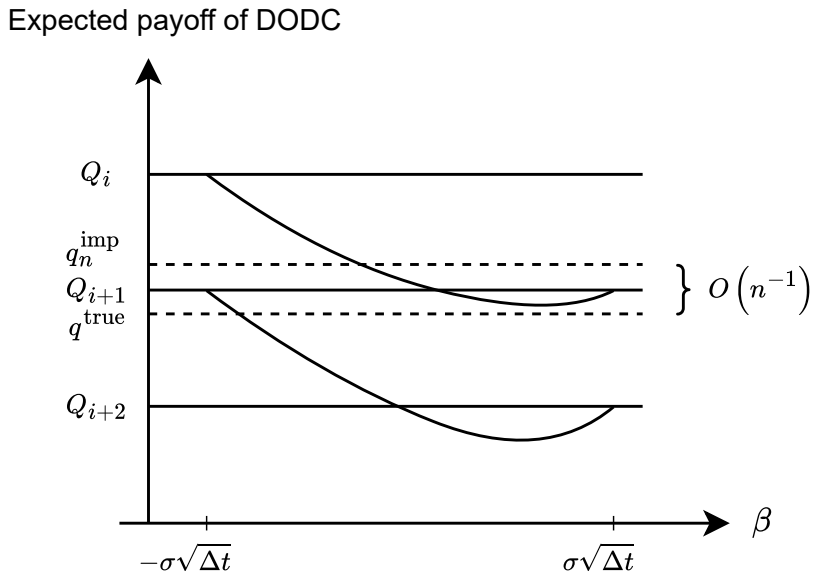

Figure 4.3: Relations among the five quantities Q_i, Q_{i+1}, Q_{i+2}, q_n^{imp}, and q^{true} for case (2).

The above inequalities imply $q_n^{\text{imp}} - q^{\text{true}} > Q_{i+1} - Q_j$, which is of order $n^{-0.5}$ for a constant barrier level, contradicting equation (4.10).

doi:10.5566/NTU2018XXXXX

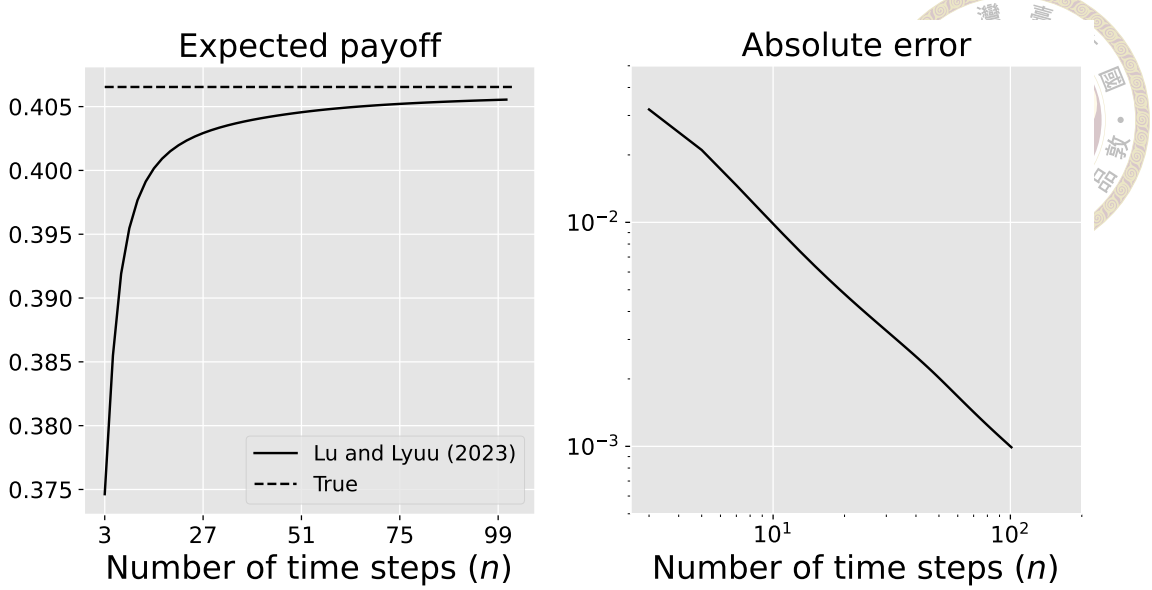

Figure 4.4: The expected payoff of a DODC and its absolute error when the barrier level is 0.9.

□

4.3 Numerical Results

The first experiment employs the n-step BTT to calculate the expected payoff of a DODC — equivalently, one minus the default probability — for $n = 3, 5, \ldots, 101$. The initial stock price is one dollar, the barrier level is 0.9, the return rate is 10%, the volatility is 25%, and the time to maturity is one year. We compare our numbers with 0.407, which is obtained by the Reiner and Rubinstein's (1991) formula. The left panel of Figure 4.4 plots the DODC's expected payoffs; the right panel plots the corresponding absolute errors. The convergence rate is clearly linear, consistent with Theorem 2.

The second experiment calculates the implied barrier by the n-step BTT. The parameters are the same as above except that the expected payoff 0.407 is given in place of the barrier level. The left panel of Figure 4.5 plots the implied barriers; the right panel plots the absolute errors of the implied barrier levels from 0.9. The convergence rate is again

doi:10.5566/NTU2018XXXXX

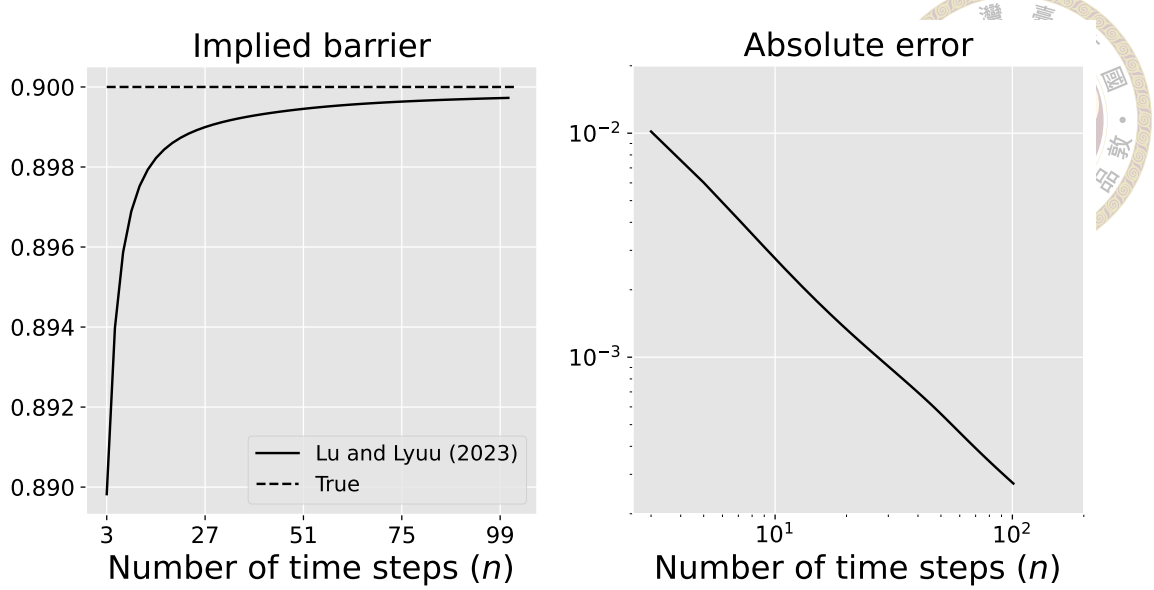

Figure 4.5: The implied barrier level and its absolute error from the true barrier level 0.9.

linear, consistent with Theorem 3.

It is interesting to see how fast the expected payoff and the implied step barrier converge even in the absence of proofs. We focus on the implied step barrier as it is built upon the expected payoff and therefore cannot better the latter's convergence rate. By concatenating twelve equal-length (thus each one month long) contiguous barriers at the same level 0.9, we effectively create a constant-barrier case for which Reiner and Rubinstein's closed-form formula again applies. The algorithm, of course, treats the barrier as a step barrier not as one single constant barrier. The parameters are otherwise the same as above. (A similar setup was used in Figure 3.7.) The left panel of Figure 4.6 shows the implied step barriers obtained for $n = 36, 156, 396, 1212$. The implied step barriers converge to the true barrier as n increases. The right panel of Figure 4.6 plots the maximum absolute errors of the implied step barriers from 0.9 for $n = 36, 60, \ldots, 1212$. The maximum absolute errors by treating the step barrier as one constant barrier are superimposed for a quick comparison. Both exhibit a linear convergence rate. The larger error in the step-barrier version compared with the constant-barrier version can be explained by the

doi:10.5566/NTU2018XXXXX

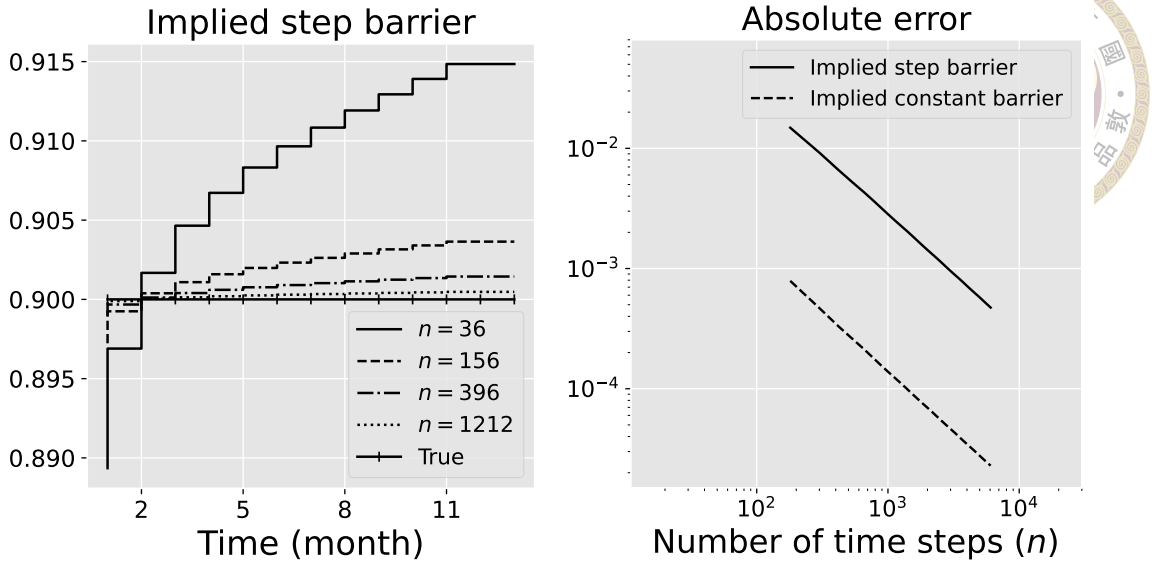

Figure 4.6: The implied step barrier and its maximum absolute error when the true step barrier consists of twelve consecutive identical barrier levels at 0.9. The absolute error by treating the step barrier as one single constant barrier is also plotted for comparison (the right panel).

fact that each of its twelve barrier levels receives only one-twelfth as many time steps as the constant-barrier version.

doi:10.5566/NTU2018XXXXX

doi:10.5566/NTU2018XXXXX

Chapter 5: Application of Implied Barrier

We use the implied barrier to develop a novel binary default prediction scheme for publicly listed companies. Furthermore, we propose a new scheme to evaluate the performance of binary default prediction schemes. Section 5.1 discusses the terminological issues in default prediction research and clarifies what constitutes a default event. Section 5.2 introduces the underlying model of our prediction scheme and Section 5.3 explains how the binary prediction scheme works. Section 5.4 elaborates on how the predictions are evaluated. We also explain related literature and compare their approaches with ours. Section 5.5 shows the experiment results of our scheme.

5.1 Bankruptcy, Failure, Financial Distress, Default, and Other Exits

Research on corporate default has been active for about 60 years. However, the terminology has not always been consistent. The same term can mean different things or the coverages of the different terms may overlap. This section briefly discusses five commonly used terms: bankruptcy, failure, financial distress, default (our focus), and other

doi:10.5566/NTU2018XXXXX

exits.

Bankruptcy is often limited to Chapter 7 or Chapter 11 filings, but [18] adds "delisting due to liquidation and poor performance" and [32] includes Chapter 10 filing. For [11], *failure* indicates "bankruptcy, bond default, an overdrawn bank account, or nonpayment of a preferred stock dividend," but [71] identifies it with Chapter 10 or Chapter 11 filings. [86] uses *financial distress* to mean a "company filing a petition for bankruptcy," In contrast, [19] use the term to include both bankruptcy and failure, where failure encompasses "bankruptcy, delisting, and receiving a D credit rating." *Default* subsumes bankruptcy, but disagreements abound beyond that. For example, default in [32] includes bankruptcy and "distressed exchange, dividend omission, . . ., missed payment events in dividend, interest, or principal," whereas [30] adds delisting.

Other exits was first proposed by [32] as one of their five types of firm exits, which are not mutually exclusive: bankruptcy, default, failure, merger and acquisition (M&A), and other exits. This category considers events such as reverse acquisition, leveraged buyout, or becoming a private company. [30] reduce these classifications to two mutually exclusive categories: default and other exits. Bankruptcy, default, and failure of [32] are lumped into default while M&A and other exits are now other exits. One notable difference is that [32] treats conservatorship as other exits, whereas [30] classify it as default. Our definition of default will follow [30].

doi:10.5566/NTU2018XXXXX

5.2 Model

We assume the firm's asset value at time t, V_t^{A}, follows the stochastic process:

$$d\ln V_t^{\mathrm{A}} = \left(\mu - \frac{1}{2}\sigma^2\right) dt + \sigma\, dW, \tag{5.1}$$

where μ is the asset's annual growth rate and σ its annualized volatility. In a first-passage-time structural model, the firm's equity value V_t^{E} can be regarded as a contingent claim on the firm's asset, analogous to a DOC (see [12]). The DOC price equals

$$\begin{aligned} V_t^{\mathrm{E}} \quad = \quad & V_t^{\mathrm{A}}\, N(a) - Ke^{-rT}\, N\left(a - \sigma\sqrt{T}\right) \\ & - V_t^{\mathrm{A}} \left(\frac{B}{V_t^{\mathrm{A}}}\right)^{2} \eta\, N(b) + Ke^{-rT} \left(\frac{B}{V_t^{\mathrm{A}}}\right)^{2\eta-2} N\left(b - \sigma\sqrt{T}\right) \\ & + R\left(\frac{B}{V_t^{\mathrm{A}}}\right)^{2\eta-1} N(c) + R\left(\frac{V_t^{\mathrm{A}}}{B}\right) N(c - 2\eta\sigma\sqrt{T}), \end{aligned} \tag{5.2}$$

where r is the risk-free interest rate, B is the constant default boundary, K represents the liabilities due at T, and R is the rebate that shareholders receive if the firm defaults. There are no other payoffs before T than the rebate. The formulas for a, b, c, and η are defined in Appendix A. [18] simplify the DOC model by assuming $R = 0$ and infer B from V_0^{E}, V_0^{A}, K, T, σ, and r. They use the difference between the book value of assets and equity for K and 10 years for T. For them, T is the maturity of the DOC and represents the expected lifespan of the company, not the maturity of debt payments nor some estimated default time. They found that the default boundary is insensitive to T with $T = 3, 5, 10, 30, 100$ (years) for companies on the NYSE, AMEX, and Nasdaq. [27] also reach the insensitive conclusion with $T = 5, 10, 20$ for public Canadian industrial firms listed on the Toronto

doi:10.5566/NTU2018XXXXX

Stock Exchange.

In contrast to [18], which infers the default boundary from a firm's equity value, we infer the default boundary from its default probabilities. Consider a firm's term structure of default probability up to T in the objective probability measure P (recall Section 2.1). By probability theory,

$$\begin{aligned} & \Pr^P \left(V_t^{\mathrm{A}} \leq B_t \quad \text{for some } t \in [0, T] \right) \\ = \quad & E^P \left[\mathbb{1} \left[\left[V_t^{\mathrm{A}} \leq B_t \quad \text{for some } t \in [0, T] \right] \right] \right]. \end{aligned} \tag{5.3}$$

Equation (5.3) gives the expected payoff under P of a DODC that pays one dollar at T if the underlying asset does not touch the default boundary at or before T and zero otherwise. There are two differences between the Brockman and Turtle's (2003) model and ours. First, our default boundary is time-varying rather than constant. For [18], the default boundary reflects contractual factors like redemption and safety covenants, or even situations such as regulatory violations. A constant default boundary is clearly oversimplifying. Second, for a DOC model like Brockman and Turtle's (2003), T represents the maturity date of the DOC at which point the firm pays off its liabilities and the remaining asset value goes to the shareholders. In contrast, our T is a horizon for default probabilities; it is not tied to any contractual payoff or termination event.

5.3 Our Default Prediction Scheme

We propose a new default prediction scheme based on the first-passage-time structural model with a default boundary. First, the default boundary is obtained as the implied step barrier inverted from a firm's default probabilities. The expected asset values are

doi:10.5566/NTU2018XXXXX

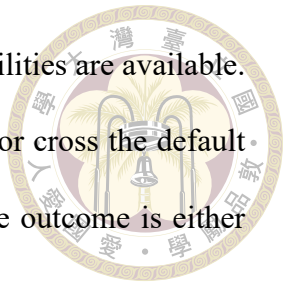

then calculated at the monitored time points where the default probabilities are available. A default signal is generated if the expected asset values ever touch or cross the default boundary from above. Our default prediction scheme is binary: The outcome is either "default" or "no-default."

Before describing the scheme in more detail, we recall the core algorithm in Section 3.1. Given m time intervals $(\,t_0, t_0+t_1\,]$, $(\,t_0+t_1, t_0+t_2\,]$, ..., $(\,t_0+t_{m-1}, t_0+t_m\,]$, the core algorithm finds the implied step barrier $[\,b_1, b_2, \ldots, b_m\,]$ that gives rise to the term structure of default probabilities $p_1, p_2, \ldots, p_m$ exactly observed at time t_0. The implied step barrier is our default boundary. We refer to t_m as the prediction horizon. In this chapter, $t_i = i$ (months) and $m = 60$.

Next, compute the expected asset values at the monitored time points t_0+1, t_0+2, ..., t_0+m as $a_1, a_2, \ldots, a_m$, respectively. To find b_1 for $(\,t_0, t_0+1\,]$, the core algorithm has a tree like Figure 2.3. To calculate the expected asset value a_1, we take the asset values of the nodes above b_1 at time t_0+1 and compute their survival probability-weighted sum. The remaining $a_2, \ldots, a_m$ are calculated likewise.

Finally, the scheme checks if the expected asset values touch or cross the default boundary as follows. For any time interval $(\,t_0+t_i, t_0+t_{i+1}\,]$, if there exists an i such that $a_i > b_i$ but $a_{i+1} \le b_{i+1}$, which means the expected asset value touches or crosses the default boundary during $(\,t_0+t_i, t_0+t_{i+1}\,]$, the scheme generates a default signal; otherwise, the scheme generates a no-default signal.

doi:10.5566/NTU2018XXXXX

5.4 Evaluation Schemes

For default prediction schemes that output a default probability, there are three major approaches to evaluating them in the literature. The first one runs a logistic regression with the default probability as the independent variable and default event as the dependent variable. The second one calculates the area under receiver operating characteristic (ROC) curve (see [32] and [30]). The third one sorts the default probabilities into, say, deciles before calculating the percentage of the firms with default events in the top decile (see [82], [18], and [21]).

Methods like logistic regression, ROC curve, and the decile approach evaluate performance using panel data in which each firm-month observation contributes one sample. Considering that default is a rare event (see [39]), the way they treat all firm-month observations as contemporaneous may boost the performance unintentionally. Take Federal Home Loan Mortgage (Freddie Mac) in the CRI dataset as an example. The dataset records 228 monthly observations and one default event from January 1991 through July 2010. For evaluation schemes that treat each firm-month observation as a distinct sample, there will be 228 samples for Freddie Mac. If a default prediction scheme simply gives no-default signals for all these 228 samples, its accuracy can appear very high, 227/228=99.6% in this case even though it fails to identify the one all-important default event. For convenience, we refer to this type of evaluation scheme as FM.

Our new evaluation scheme is firm-centric, which will be called the FC scheme throughout this chapter. Instead of treating each monthly signal of a binary default prediction scheme as a distinct sample, the entire sequence of monthly signals for a firm determines whether the FC scheme makes the correct call about the firm. The main ad-

doi:10.5566/NTU2018XXXXX

vantage of this approach is that it alleviates the extreme imbalance in numbers between the default and non-default events by making each firm contribute only one sample to the performance metrics regardless of its number of monthly observations, most of which have no default events at all. In fact, the firm-centric approach suits a binary default scheme better when dealing with rare events (this point will be elaborated upon shortly).

The FC scheme works as follows. First, it runs our default prediction scheme for each firm observed at times $t_0 = t_s, t_s + 1, t_s + 2, \ldots, t_e$, where t_s is the first time point the firm has an entry in the dataset and t_e is the last. All classifications will be based on the prediction signals and the real events recorded in the dataset within $[\, t_s, t_e + 60\,]$. We treat $[\, t_e + 1, t_e + 60\,]$ as if the dataset recorded no default events in this extended time interval.

Next, each firm is categorized into one of four groups for statistical analysis as follows. If a firm books a default event in the dataset, a correct call for the firm means the first default event happens within the prediction horizon of the first default signal, which will be labeled as a true positive (TP). If a firm never defaults, a correct call for the firm means the default prediction scheme generates only no-default signals, which will be labeled as a true negative (TN). All the other scenarios are considered wrong calls. A false positive (FP) occurs when (1) the firm never defaults but a default signal is generated at least once, (2) the firm defaults before the first default signal, or (3) the firm defaults after the prediction horizon of the first default signal. A false negative (FN) occurs if the firm books a default event in the dataset but the default prediction scheme generates only no-default signals. To the best of our knowledge, our evaluation scheme is the first of its kind. The key characteristic of it is that the default prediction scheme makes a wrong call for a firm with just one single wrong prediction over the period of time the firm is being

doi:10.5566/NTU2018XXXXX

tracked.

After each firm is classified, we calculate four common performance metrics: accuracy, precision, recall, and the F1 score. They are defined as

$$\begin{aligned} \text{accuracy} &= \frac{\text{TP}+\text{TN}}{\text{TP}+\text{FP}+\text{FN}+\text{TN}}, \\ \text{precision} &= \frac{\text{TP}}{\text{TP}+\text{FP}}, \\ \text{recall} &= \frac{\text{TP}}{\text{TP}+\text{FN}}, \\ \text{F1} &= 2 \times \frac{\text{precision} \times \text{recall}}{\text{precision}+\text{recall}}, \end{aligned}$$

respectively (see [37]). Accuracy refers to the proportion of correct calls among all the firms. Precision measures the percentage of correct calls among firms receiving default signals. Recall measures the percentage of correct calls among firms with default events. The F1 score, the harmonic mean of precision and recall, offers a balanced assessment of a model's predictive performance.

We now analyze a typical FM scheme's TP, TN, FP, FN, and the above four performance metrics compared with our FC scheme's. Now every monthly signal contributes one to exactly one of the TP, TN, FP, and FN counts as follows:

1. For each TP by the FC scheme, scheme FM adds one to TP and the number of monthly observations before the first default signal to TN. The former is true because TP occurs only in the month when our default prediction scheme generates the first default signal. The latter is true because our default prediction scheme must have generated consecutive monthly no-default signals before then and they are all

doi:10.5566/NTU2018XXXXX

correct.

2. For each TN by the FC scheme, scheme FM adds the number of monthly observations in the dataset to TN. This is because this many months have neither default events nor default signals.

3. For each FP by the FC scheme, scheme FM adds one to FP and the number of monthly observations before the first default signal to TN. The former is true because FP occurs only in the month when our default prediction scheme generates the first default signal. The latter is true for the same reason as in the case of TP.

4. For each FN by the FC scheme, scheme FM adds one to FN and the number of monthly observations before the first default event to TN. The former is true because FN occurs only in the month when the default event happens. The latter follows the convention in the case of TP.

Note that only the TN count is affected when switching from FC to FM. As a result, only accuracy is changed among the four performance metrics because it is the only one that takes TN into consideration.

Let TN_{FM} and $\text{accuracy}_{\text{FM}}$ denote the values of TN and accuracy under scheme FM. Hence

$$\begin{aligned}
\text{TN}_{\text{FM}} &= \begin{pmatrix}\text{Avg. number of monthly observations before}\\ \text{the first default signal per TP of the FC scheme}\end{pmatrix} \times \text{TP} \\
&+ \begin{pmatrix}\text{Avg. number of monthly observations}\\ \text{in the dataset per TN of the FC scheme}\end{pmatrix} \times \text{TN} \\
&+ \begin{pmatrix}\text{Avg. number of monthly observations before}\\ \text{the first default signal per FP of the FC scheme}\end{pmatrix} \times \text{FP} \\
&+ \begin{pmatrix}\text{Avg. number of monthly observations before}\\ \text{the first default event per FN of the FC scheme}\end{pmatrix} \times \text{FN} \qquad (5.4)
\end{aligned}$$

$$\text{accuracy}_{\text{FM}} = \frac{\text{TP} + \text{TN}_{\text{FM}}}{\text{TP} + \text{FP} + \text{FN} + \text{TN}_{\text{FM}}}. \qquad (5.5)$$

doi:10.5566/NTU2018XXXXX

That defaults are rare has two implications for any large and representative dataset. First, firms with no default events typically stay in the dataset for many months, which means that the coefficient of TN in formula (5.4) is large.[1] Second, TN is usually orders of magnitude greater than TP, FP, and FN. These two observations together indicate that TN_{FM} dominates TP, TN, FP, and FN. As a result, $\text{accuracy}_{\text{FM}}$ will be close to 100% by formula (5.5). Take the CRI dataset as an example. When the prediction horizon is 60 months, $\text{TP} = 499$, $\text{TN} = 14620$, $\text{FP} = 334$, $\text{FN} = 526$, and $\text{accuracy} = 92.39\%$. In comparison, $\text{TN}_{\text{FM}} = 1755358$ and $\text{accuracy}_{\text{FM}} = 99.95\%$, which is very close to 100%. Our FC scheme clearly does not give a misleadingly high accuracy as the FM scheme.

The final task is to compare our default prediction scheme with the default-probability-based ones. Because the latter are not binary, the first step is to decide a threshold θ for the predicted default probabilities such that a "default" signal is generated whenever the probability exceeds θ. The θ is determined by a grid search from 0.01 to 0.99 such that the F1 score is maximized. Note that θ depends on the prediction horizon and all the firm-month observations in the dataset. We call this the prescient default prediction scheme because it uses future information. In contrast, our default prediction scheme does not see the future.

5.5 Experiments

Our data are provided by the Credit Research Initiative (CRI) of the National University of Singapore (recall Section 3.3). We work on all the companies listed on the NYSE, AMEX and Nasdaq. All are U.S. exchanges because the U.S. capital market is efficient

[1] For the CRI dataset, the average number is 109.82 months.

doi:10.5566/NTU2018XXXXX

and a more uniform legal code applies when only a single nation is covered. The data are monthly and span over 390 months, from January 1991 through June 2023. There are 16,873 firms and 1,914,494 firm-month observations in total. For each firm-month observation, we have (1) $p_1, p_2, \cdots, p_{60}$, the term structure of the default probabilities up to 60 months, (2) μ, the annual growth rate of the firm's asset, and (3) σ, the annualized volatility of the firm's asset. To calculate the default boundary, we need the above three variables and the initial asset value.

For structural models, the default event is triggered when the asset value touches the default boundary. So what matters is the asset values relative to the default boundary. The default probabilities remain unchanged under our constant-parameter model (5.1) for any rescaling of V_t^{A} and B_t in equation (5.3). Therefore, we assume a firm's initial asset value is one dollar or $V_0^{\mathrm{A}} = 1$. Under this convention, the asset value and the default boundary are both relative to the initial asset value.

Table 5.1 reports the summary statistics of the dataset. Default probabilities are cumulative. For example, a 3-month default probability refers to the probability of a default event over the ensuing 3 months, and a 6-month default probability refers to the probability of a default event over the ensuing 6 months, both starting from now. Obviously, the default probabilities increase with time. We observe that default probabilities are small in general. Take the 12-month default probability in Table 5.1 as an example. The mean and median are 0.865% and 0.100%, respectively. Even for the 60-month case, the mean and median are only 3.575% and 1.947%, respectively. The distributions of default probabilities are positively skewed because the median is consistently smaller than the mean. This implies that a small number of firms have much higher default probabilities than the majority. This positive skewness applies to annual asset growth rates and annual asset

doi:10.5566/NTU2018XXXXX

Table 5.1: Summary statistics of all firm-month data. The firms are all publicly listed on NYSE, AMEX, and Nasdaq. For brevity, we list only the cumulative default probabilities at 1, 3, 6, 12, 24, 36, 48, and 60 months. All the numbers are in percentage.

	Mean	Standard deviation	Minimum	Median	Maximum
p_1	0.061	0.734	0.000	0.001	89.350
p_3	0.193	1.678	0.000	0.006	99.737
p_6	0.410	2.594	0.000	0.021	99.871
p_{12}	0.865	3.635	0.000	0.100	99.872
p_{24}	1.697	4.585	0.000	0.433	99.872
p_{36}	2.404	5.047	0.000	0.901	99.872
p_{48}	3.024	5.330	0.000	1.422	99.872
p_{60}	3.575	5.524	0.000	1.947	99.872
μ	−4.527	62.542	−2247.233	−0.800	4163.562
σ	49.611	54.924	4.460	35.241	2891.924

volatilities as well. This is consistent with prior studies (see [35]).

5.5.1 The CRI Dataset: Default Events and Summary Statistics

Recall that our terminology follows [30]. There are 13,789 credit events in the dataset from January 1991 through June 2023. Among them, 1,595 are default events and 12,194 are other exits. The default events consist of three cases: (1) Companies filing for bankruptcy under Chapter 7, 11, or 15 of the United States bankruptcy code, (2) companies missing payments in coupon, interest, loan, or principal, and (3) companies that are taken into conservatorship of the United States government. Other exits include merger and acquisition or failure to meet the listing requirements, among others.[2] The summary statistics of the annual firm count and default count appear in Table 5.2. A firm is counted as active in a year if it has at least one firm-month observation in that year.

Figure 5.1 plots the numbers of publicly listed companies in the U.S. per year from

[2]Please refer to https://d.nuscri.org/static/pdf/Technicalreport_2023.pdf for the full detail.

doi:10.5566/NTU2018XXXXX

Table 5.2: Numbers of active companies listed on NYSE, AMEX, and Nasdaq and their default events per year during 1991–2023. A firm is counted as active if it has at least one firm-month observation in that year.

Year	# of active firm	# of default events (% of default events)	Year	# of active firm	# of default events (% of default events)
1991	3628	18 (0.496%)	2008	4980	57 (1.145%)
1992	4563	16 (0.351%)	2009	4621	96 (2.077%)
1993	5395	27 (0.500%)	2010	4428	27 (0.610%)
1994	6279	16 (0.255%)	2011	4277	31 (0.725%)
1995	6746	16 (0.237%)	2012	4195	37 (0.882%)
1996	7289	17 (0.233%)	2013	4184	21 (0.502%)
1997	7669	48 (0.626%)	2014	4279	24 (0.561%)
1998	7829	73 (0.932%)	2015	4393	46 (1.047%)
1999	7485	80 (1.069%)	2016	4300	78 (1.814%)
2000	7210	103 (1.429%)	2017	4223	46 (1.089%)
2001	6608	172 (2.603%)	2018	4225	26 (0.615%)
2002	5919	108 (1.825%)	2019	4225	43 (1.018%)
2003	5520	77 (1.395%)	2020	4239	84 (1.982%)
2004	5326	37 (0.695%)	2021	4924	22 (0.447%)
2005	5307	35 (0.660%)	2022	5060	23 (0.455%)
2006	5243	20 (0.381%)	2023	4793	47 (0.981%)
2007	5220	24 (0.460%)			

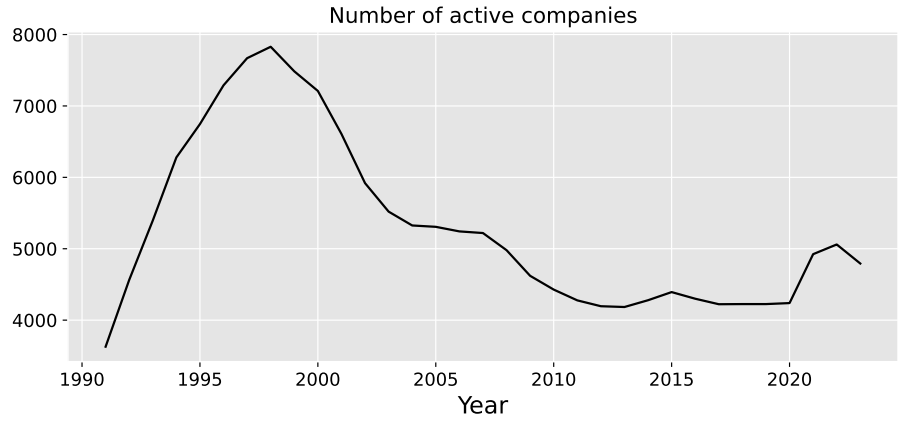

Figure 5.1: Number of active companies per year on NYSE, AMEX, and Nasdaq from 1991 through 2023.

Table 5.2. A downward trend started around 1998. [28] find that the high delisting rate can be attributed to a high rate of M&A, which may also explain why there are so many other exits compared with default events in the CRI dataset. Since not all exits are caused by financial distress, a precise definition for "default" is critical before evaluating a default prediction scheme (recall Section 5.1).

Figure 5.2 plots the number of default events per year. The four peak points, in 2001,

doi:10.5566/NTU2018XXXXX

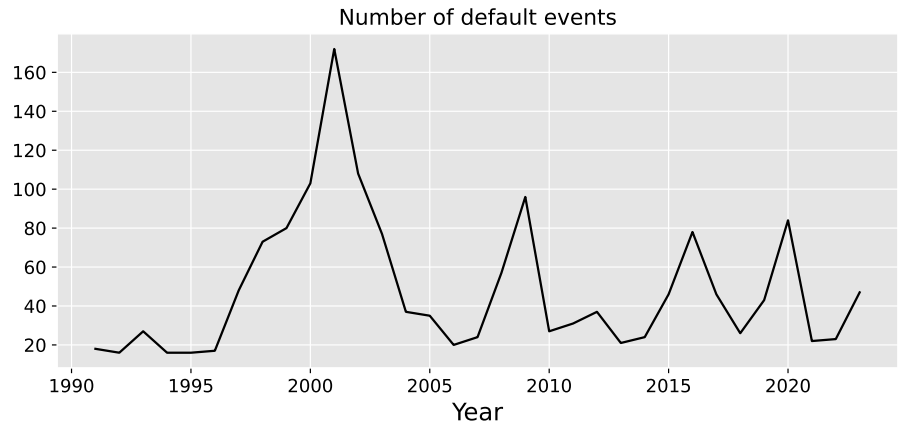

Figure 5.2: Number of default events per year from 1991 to 2023.

2009, 2016, and 2020, can be attributed to the dot-com bubble, the global financial crisis, the Chinese market crash (see [1]), and the US-China trade war (see [42]), respectively. Interestingly, these four crises started one year earlier in 2000, 2008, 2015, and 2019, respectively. They show that default events arise rapidly about one year after the financial downturn commenced. The upward trend at the end of the figure indicates a new wave of default events, which may be caused by COVID-19.

5.5.2 Default boundary

As an illustration, Figure 5.3 depicts the default boundary of Freddie Mac as of May 2008 with 60 barrier levels. The x-axis represents the number of months from that date, and the y-axis is the default boundary. For example, the default boundary is about 56.4% of the initial asset value in month 7. So the expected asset value will touch the default boundary if it loses 43.6% of its initial asset value in December 2008.

doi:10.5566/NTU2018XXXXX

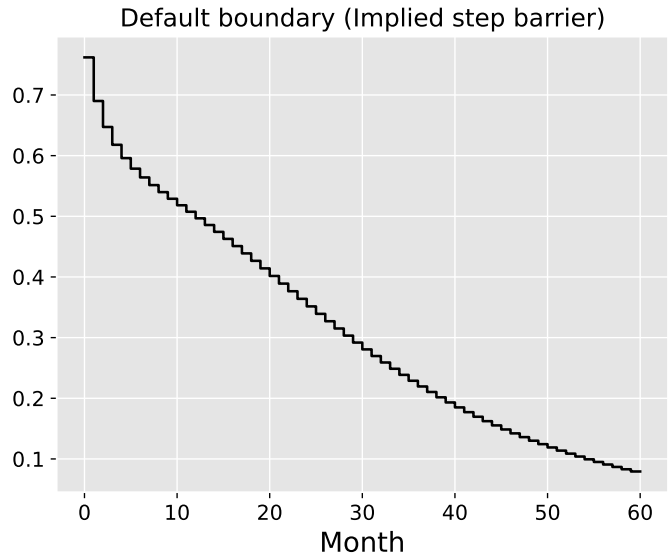

Figure 5.3: Default boundary of Freddie Mac as of May 2008.

5.5.3 Evaluation: The Firm-Centric Approach

Each firm has many monthly observations. Our default prediction scheme generates expected asset values, the default boundaries, and the signals (defaults or no-defaults) from them. We use Freddie Mac as an example to explain how the FC scheme makes the call about this firm (see Figure 5.4). Our prediction scheme generates default signals in June, July, August, and September of 2008. Since the first default event, which is in September 2008, happens within 5 years of our first default signal, the firm counts as a TP.

Table 5.3 shows the performance metrics of our default prediction scheme and the prescient default prediction scheme when both are evaluated by the FC scheme. The prediction horizons are 3, 6, 12, 36, and 60 months. The thresholds for the prescient scheme in the table are obtained by maximizing the F1 score among 0.01, 0.02, $\cdots$, 0.99, and 1 (see Section 5.4). For example, a default signal for the 12-month prediction horizon is generated in the prescient scheme if $p_{12} > 0.34$.

doi:10.5566/NTU2018XXXXX

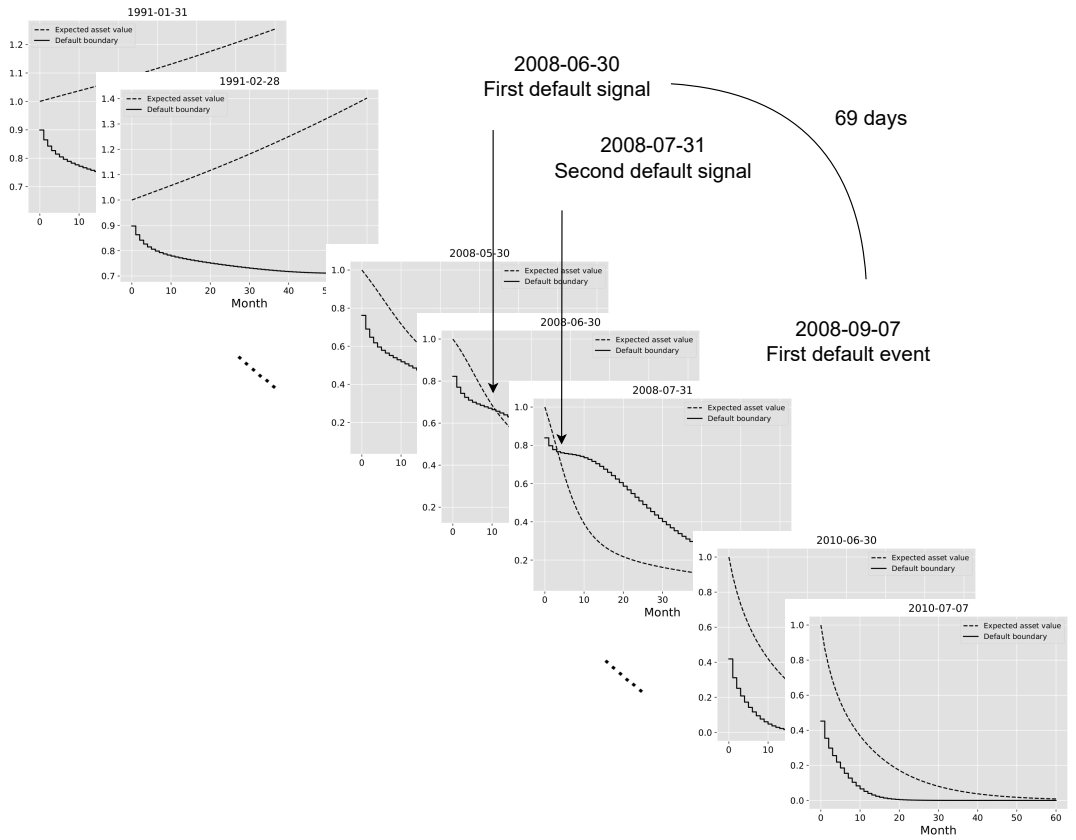

Figure 5.4: Signals from our default prediction scheme for Freddie Mac. The dashed lines are the expected asset values. The solid lines are the default boundaries.

In Table 5.3, our prediction scheme's accuracies are superior across all prediction horizons even when pitted against the prescient scheme that uses future information. Although the large TN relative to TP, FP, and FN makes all accuracies higher than 90%, those from the FC scheme remain discriminative being between 90.54% and 92.39%. Had we used the FM scheme, the accuracies of both default prediction schemes would have been close to 100%, making the metric useless in practice. Next, we discuss precision and recall together because their formulas are similar. Their only difference lies in the denominators: Precision uses TP + FP, while recall uses TP + FN. Between two reasonably good default prediction schemes, the one that generates fewer default signals tends to have lower FP and higher FN; as a result, precision tends to be higher and recall tends to be lower. This trade-off has been documented before (see [67]). In Table 5.3, our scheme consistently

doi:10.5566/NTU2018XXXXX

Table 5.3: Performance metrics. The Ours columns show the results of our default prediction scheme. The P columns show the results of the prescient default prediction scheme. Boldfaced numbers signify the outperformers. The prediction horizons are in months. Accuracy, precision, recall, and the F1 score are in percentage.

Prediction horizon	3		6		12		36		60	
	Ours	P	Ours	P	Ours	P	Ours	P	Ours	P
Threshold for P		0.14		0.21		0.34		0.42		0.43
Accuracy	**91.51**	90.77	**91.96**	90.54	**92.14**	91.08	**92.34**	91.12	**92.39**	91.09
Precision	39.38	**41.37**	**50.14**	44.84	**54.26**	48.09	**58.94**	48.97	**59.90**	48.86
Recall	15.95	**45.05**	26.80	**54.03**	32.40	**53.82**	35.00	**55.21**	35.36	**55.70**
F1	22.70	**43.13**	34.93	**48.79**	40.57	**50.79**	43.92	**51.90**	44.47	**52.05**

exhibits higher precision but lower recall and F1 score than the prescient scheme across all prediction horizons. This suggests that our prediction scheme is more conservative in generating default signals. Therefore, its default signals are more likely to be correct.

doi:10.5566/NTU2018XXXXX

doi:10.5566/NTU2018XXXXX

References

[1] A. D. Ahmed and R. Huo. Impacts of China's Crash on Asia-Pacific Financial Integration: Volatility Interdependence, Information Transmission and Market Co-movement. Economic Modelling, 79:28–46, 2019.

[2] E. I. Altman. Financial Ratios, Discriminant Analysis and the Prediction of Corporate Bankruptcy. Journal of Finance, 23(4):589–609, 1968.

[3] E. I. Altman. Fifty Years of Z-Scores To Predict the Probability of Corporate Bankruptcy. Journal of Investment Consulting, 19(1):15–22, 2019.

[4] R. W. Anderson and S. Sundaresan. Design and Valuation of Debt Contracts. Review of Financial Studies, 9(1):37–68, 1996.

[5] R. W. Anderson, S. Sundaresan, and P. Tychon. Strategic Analysis of Contingent Claims. European Economic Review, 40(3):871–881, 1996.

[6] G. F. Armstrong. Valuation Formulae for Window Barrier Options. Applied Mathematical Finance, 8(4):197–208, 2001.

[7] K. E. Atkinson. An Introduction to Numerical Analysis. John Wiley & Sons, New York, 2 edition, 1989.

[8] T. Atkinson, D. Luttrell, and H. Rosenblum. Assessing the Costs and Consequences

doi:10.5566/NTU2018XXXXX

of the 2007–09 Financial Crisis and Its Aftermath. Economic Letter, 8(7), September 2013.

[9] M. Avellaneda and J. Zhu. Distance to Default. Risk, 14(12):125–129, 2001.

[10] F. Barboza, H. Kimura, and E. Altman. Machine Learning Models and Bankruptcy Prediction. Expert Systems with Applications, 83:405–417, 2017.

[11] W. H. Beaver. Financial Ratios as Predictors of Failure. Journal of Accounting Research, 4:71–111, 1966.

[12] F. Black and J. C. Cox. Valuing Corporate Securities: Some Effects of Bond Indenture Provisions. Journal of Finance, 31(2):351–367, 1976.

[13] F. Black and M. Scholes. The Pricing of Options and Corporate Liabilities. Journal of Political Economy, 81(3):637–654, 1973.

[14] C. Bluhm, L. Overbeck, and C. Wagner. Introduction to Credit Risk Modeling. Financial Mathematics Series. Chapman & Hall/CRC, Boca Raton, FL, 2nd edition, 2010.

[15] D. Bonfim. Credit Risk Drivers: Evaluating the Contribution of Firm Level Information and of Macroeconomic Dynamics. Journal of Banking & Finance, 33(2):281–299, 2009.

[16] P. P. Boyle and S. H. Lau. Bumping Up against the Barrier with the Binomial Method. Journal of Derivatives, 1(4):6–14, 1994.

[17] M. Broadie, P. Glasserman, and S.-G. Kou. A Continuity Correction for Discrete Barrier Options. Mathematical Finance, 7(4):325–348, 1997.

doi:10.5566/NTU2018XXXXX

[18] P. Brockman and H. J. Turtle. A Barrier Option Framework for Corporate Security Valuation. Journal of Financial Economics, 67(3):511–529, 2003.

[19] J. Campbell, J. Hilscher, and J. Szilagyi. In Search of Distress Risk. Journal of Finance, 63(6):2899–2939, 2008.

[20] L.-B. Chang and K. Palmer. Smooth Convergence in the Binomial Model. Finance and Stochastics, 11(1):91–105, 2007.

[21] S. Chava and R. A. Jarrow. Bankruptcy Prediction with Industry Effects. Review of Finance, 8(4):537–569, 2004.

[22] C.-Y. Chen, P.-J. Chou, Y.-S. Hsu, P.-H. Liu, Y.-D. Lyuu, and C.-J. Wang. A Closed-Form Formula for an Option with Discrete and Continuous Barriers. Communications in Statistics — Theory and Methods, 40(2):345–357, 2010.

[23] T. H. Cormen, C. E. Leiserson, R. L. Rivest, and C. Stein. Introduction to Algorithms. MIT Press, Cambridge, MA, 3 edition, 2009.

[24] J. C. Cox, S. A. Ross, and M. Rubinstein. Option Pricing: A Simplified Approach. Journal of Financial Economics, 7(3):229–263, 1979.

[25] P. J. Crosbie and J. R. Bohn. Modeling Default Risk, volume 2, pages 471–506. World Scientific, 2019.

[26] T.-S. Dai and Y.-D. Lyuu. The Bino-Trinomial Tree: A Simple Model for Efficient and Accurate Option Pricing. Journal of Derivatives, 17(4):7–24, 2010.

[27] G. Dionne and S. Laajimi. On the Determinants of the Implied Default Barrier. Journal of Empirical Finance, 19(3):395–408, 2012.

doi:10.5566/NTU2018XXXXX

[28] C. Doidge, G. A. Karolyi, and R. M. Stulz. The U.S. Listing Gap. Journal of Financial Economics, 123(3):464–487, 2017.

[29] P. F. Drucker. Management: Tasks, Responsibilities, Practices. Harper & Row, New York, 1974.

[30] J.-C. Duan, J. Sun, and T. Wang. Multiperiod Corporate Default Prediction —A Forward Intensity Approach. Journal of Econometrics, 170(1):191–209, 2012.

[31] D. Duffie. Dynamic Asset Pricing Theory. Princeton University Press, Princeton, NJ, 2 edition, 1996.

[32] D. Duffie, L. Saita, and K. Wang. Multi-period Corporate Default Prediction with Stochastic Covariates. Journal of Financial Economics, 83(3):635–665, 2007.

[33] D. Duffie and K. Singleton. Modeling Term Structure of Defaultable Bonds. Review of Financial Studies, 12(4):687–720, 1999.

[34] D. Duffie and K. J. Singleton. Credit Risk: Pricing, Measurement, and Management. Princeton University Press, Princeton, NJ, 2003.

[35] A. Farago and E. Hjalmarsson. Long-Horizon Stock Returns Are Positively Skewed. Review of Finance, 27(2):495–538, 2022.

[36] S. Figlewski and B. Gao. The Adaptive Mesh Model: A New Approach to Efficient Option Pricing. Journal of Financial Economics, 53(3):313–351, 1999.

[37] I. Goodfellow, Y. Bengio, and A. Courville. Deep Learning. MIT Press, Cambridge, MA, 2016.

[38] J. R. Graham. How Big Are the Tax Benefits of Debt? Journal of Finance, 55(5):1901–1941, 2000.

doi:10.5566/NTU2018XXXXX

[39] S. Hanson and T. Schuermann. Confidence Intervals for Probabilities of Default. Journal of Banking & Finance, 30(8):2281–2301, 2006.

[40] R. C. Heynen and H. M. Kat. Partial Barrier Options. Journal of Financial Engineering, 3(3):253–274, 1994.

[41] S. A. Hillegeist, E. K. Keating, D. P. Cram, and K. G. Lundstedt. Assessing the Probability of Bankruptcy. Review of Accounting Studies, 9(1):5–34, 2004.

[42] Y. Huang, C. Lin, S. Liu, and H. Tang. Trade Networks and Firm Value: Evidence from the U.S.-China Trade War. Journal of International Economics, 145:103811, 2023.

[43] C.-H. Hui. Time Dependent Barrier Option Values. Journal of Futures Markets, 17(6):667–688, 1997.

[44] J. Hull. Options, Futures, and Other Derivatives. Pearson Prentice Hall, Upper Saddle River, NJ, 6 edition, 2006.

[45] J. Hull and A. White. Valuing Credit Default Swaps II: Modeling Default Correlations. Journal of Derivatives, 8(3):12–22, 2001.

[46] A. C. Ian and A. D. Sergei. Estimating the Cost of Risky Debt. Journal of Applied Corporate Finance, 19(3):90–95, 2007.

[47] J. E. Ingersoll. Theory of Financial Decision Making. Rowman & Littlefield, Totowa, NJ, 1987.

[48] R. Jarrow, D. Lando, and S. M. Turnbull. A Markov Model for the Term Structure of Credit Risk Spreads. Review of Financial Studies, 10(2):481–523, 1997.

doi:10.5566/NTU2018XXXXX

[49] R. Jarrow and S. M. Turnbull. Pricing Derivatives on Financial Securities Subject to Credit Risk. Journal of Finance, 50(1):53–85, 1995.

[50] J. Jájá. An Introduction to Parallel Algorithms. Addison-Wesley, Redwood, CA, 1992.

[51] I. J. Kim, K. Ramaswamy, and S. Sundaresan. Does Default Risk in Coupons Affect the Valuation of Corporate Bonds?: A Contingent Claims Model. Financial Management, 22(3):117–131, 1993.

[52] S.-G. Kou. On Pricing of Discrete Barrier Options. Statistica Sinica, 13(4):955–964, 2003.

[53] N. Kunitomo and M. Ikeda. Pricing Options With Curved Boundaries. Mathematical Finance, 2(4):275–298, 1992.

[54] D. Lando. Credit Risk Modeling: Theory and Applications. Princeton University Press, Princeton, NJ, 2004.

[55] G. Leduc and K. Palmer. What a Difference One Probability Makes in the Convergence of Binomial Trees. International Journal of Theoretical and Applied Finance, 23:1–26, 2020.

[56] G. Leduc and K. Palmer. The Convergence Rate of Option Prices in Trinomial Trees. Risks, 11:1–33, 2023.

[57] H. Lee, G. Lee, and S. Song. Multi-Step Reflection Principle and Barrier Options. Journal of Future Markets, 42(4):692–721, 2022.

[58] H. E. Leland and K. B. Toft. Optimal Capital Structure, Endogenous Bankruptcy, and the Term Structure of Credit Spreads. Journal of Finance, 51(3):987–1019, 1996.

doi:10.5566/NTU2018XXXXX

[59] J.-R. Lin and K. Palmer. Convergence of Barrier Option Prices in the Binomial Model. Mathematical Finance, 23(2):318–338, 2013.

[60] R. Litterman and T. Iben. Corporate Bond Valuation and the Term Structure of Credit Spreads. Journal of Portfolio Management, 17(3):52–64, 1991.

[61] L.-C. Liu, T.-S. Dai, and C.-J. Wang. Evaluating Corporate Bonds and Analyzing Claim Holders' Decisions with Complex Debt Structure. Journal of Banking & Finance, 72:151–174, 2016.

[62] U. H. L. Lok and Y.-D. Lyuu. Efficient Trinomial Trees for Local-Volatility Models in Pricing Double-Barrier Options. Journal of Futures Markets, 40(4):556–574, 2020.

[63] F. A. Longstaff and E. S. Schwartz. A Simple Approach to Valuing Risky Fixed and Floating Rate Debt. Journal of Finance, 50(3):789–819, 1995.

[64] Y.-D. Lyuu. Very Fast Algorithms for Barrier Option Pricing and the Ballot Problem. Journal of Derivatives, 5(3):68–79, 1998.

[65] Y.-D. Lyuu. Financial Engineering & Computation: Principles, Mathematics, Algorithms. Cambridge University Press, Cambridge, 2002.

[66] Y.-D. Lyuu and Y.-Q. Zhang. Pricing Multi-Asset Time-Varying Double-Barrier Options with Time-Dependent Parameters. Journal of Futures Markets, 43(3):404–434, 2023.

[67] C. D. Manning, P. Raghavan, and H. Schütze. Introduction to Information Retrieval. Cambridge University Press, Cambridge, UK, 2008.

doi:10.5566/NTU2018XXXXX

[68] D. Martin. Early Warning of Bank Failure: A Logit Regression Approach. Journal of Banking & Finance, 1(3):249–276, 1977.

[69] R. C. Merton. On the Pricing of Corporate Debt: The Risk Structure of Interest Rates. Journal of Finance, 29(2):449–470, 1974.

[70] J. Nickerson and J. M. Griffin. Debt Correlations in the Wake of the Financial Crisis: What Are Appropriate Default Correlations for Structured Products? Journal of Financial Economics, 125(3):454–474, 2017.

[71] J. A. Ohlson. Financial Ratios and the Probabilistic Prediction of Bankruptcy. Journal of Accounting Research, 18(1):109–131, 1980.

[72] K. G. Palepu. Predicting Takeover Targets: A Methodological and Empirical Analysis. Journal of Accounting and Economics, 8(1):3–35, 1986.

[73] E. Reiner. Breaking Down the Barriers. Risk, 4(8):28–35, 1991.

[74] E. Reiner and M. Rubinstein. Unscrambling the Binary Code. Risk, 4(9):75–83, 1991.

[75] P. Ritchken. On Pricing Barrier Options. Journal of Derivatives, 3(2):19–28, 1995.

[76] L. G. C. Rogers and O. Zane. Valuing Moving Barrier Options. Journal of Computational Finance, 1(1):5–11, 1997.

[77] M. Scheffer. Critical Transitions in Nature and Society. Princeton University Press, Princeton, NJ, 2009.

[78] M. Scheffer, J. Bascompte, W. A. Brock, V. Brovkin, S. R. Carpenter, V. Dakos, H. Held, E. H. van Nes, M. Rietkerk, and G. Sugihara. Early-Warning Signals for Critical Transitions. Nature, 461(7260):53–59, 2009.

doi:10.5566/NTU2018XXXXX

[79] P. V. Shevchenko. Addressing the Bias in Monte Carlo Pricing of Multi-Asset Options with Multiple Barriers through Discrete Sampling. Journal of Computational Finance, 6(3):1–20, 2003.

[80] R. J. Shiller. Irrational Exuberance. Princeton University Press, Princeton, NJ, 2 edition, 2009.

[81] S. E. Shreve. Stochastic Calculus for Finance I: The Binomial Asset Pricing Model. Springer, New York, 2004.

[82] T. Shumway. Forecasting Bankruptcy More Accurately: A Simple Hazard Model. Journal of Business, 74(1):101–124, 2001.

[83] J. B. Walsh. The Rate of Convergence of the Binomial Tree Scheme. Finance and Stochastics, 7:337–361, 2003.

[84] C.-J. Wang, T.-S. Dai, and Y.-D. Lyuu. Evaluating Corporate Bonds with Complicated Liability Structures and Bond Provisions. European Journal of Operational Research, 237(2):749–757, 2014.

[85] C. Zhou. The Term Structure of Credit Spreads with Jump Risk. Journal of Banking & Finance, 25(11):2015–2040, 2001.

[86] M. E. Zmijewski. Methodological Issues Related to the Estimation of Financial Distress Prediction Models. Journal of Accounting Research, 22:59–82, 1984.

doi:10.5566/NTU2018XXXXX

doi:10.5566/NTU2018XXXXX

Appendix A — Validity of Branching Probabilities

To prove P_u, P_m, and P_d are valid probabilities, it suffices to prove $P_u, P_m, P_d \geq 0$. We know Δ is negative in formula (2.13). This means Δ_u, Δ_m, and Δ_d in formulas (2.14)–(2.16) must be non-positive or, equivalently, $\beta\gamma + \text{Var} \geq 0$, $\alpha\gamma + \text{Var} \leq 0$, and $\alpha\beta + \text{Var} \geq 0$. From formulas (2.14)–(2.16) and inequalities (2.9), we have

$$\begin{aligned} \beta\gamma + \text{Var} &= \beta^2 - 2\beta\sigma\sqrt{\Delta t} + \sigma^2\Delta t \\ &= \left(\beta - 2\sigma\sqrt{\Delta t}\right)^2 \geq 0, \qquad \text{(A.6)} \\ \alpha\gamma + \text{Var} &= \beta^2 - 4\sigma^2\Delta t + \sigma^2\Delta t \\ &= \beta^2 - 3\sigma^2\Delta t \leq 0, \qquad \text{(A.7)} \\ \alpha\beta + \text{Var} &= \beta^2 + 2\beta\sigma\sqrt{\Delta t} + \sigma^2\Delta t \\ &= \left(\beta + 2\sigma\sqrt{\Delta t}\right)^2 \geq 0, \qquad \text{(A.8)} \end{aligned}$$

as desired (see [26]).

doi:10.5566/NTU2018XXXXX

doi:10.5566/NTU2018XXXXX

Chapter A: Values of a, b, c, and η in Equation (5.2)

$$a = \begin{cases} \frac{\ln\frac{V_t^{\mathrm{A}}}{K}+(r+\frac{1}{2}\sigma^2)T}{\sigma\sqrt{T}}, & \text{if } B \geq K. \\ \frac{\ln\frac{V_t^{\mathrm{A}}}{B}+(r+\frac{1}{2}\sigma^2)T}{\sigma\sqrt{T}}, & \text{if } B < K. \end{cases} \tag{A.1}$$

$$b = \begin{cases} \frac{\ln\frac{B^2}{V_t^{\mathrm{A}}K}+(r+\frac{1}{2}\sigma^2)T}{\sigma\sqrt{T}}, & \text{if } B \geq K. \\ \frac{\ln\frac{B}{V_t^{\mathrm{A}}}+(r+\frac{1}{2}\sigma^2)T}{\sigma\sqrt{T}}, & \text{if } B < K. \end{cases} \tag{A.2}$$

$$c = \frac{\ln\frac{B}{V_t^{\mathrm{A}}} + (r+\frac{1}{2}\sigma^2)T}{\sigma\sqrt{T}}. \tag{A.3}$$

$$\eta = \frac{r}{\sigma^2} + \frac{1}{2}. \tag{A.4}$$

doi:10.5566/NTU2018XXXXX